ATP hydrolysis kinetics and thermodynamics as determinants of calcium oscillation in pancreatic β cells

Yunsheng Sun,* Dianjie Li,* Congjian Ni, and Yingda Ge
School of Physics, Peking University, Beijing 100871, China

Hong Qian
Department of Applied Mathematics, University of Washington, Seattle, Washington 98195, USA

Qi Ouyang and Fangting Li†
School of Physics, Peking University, Beijing 100871, China
and Center for Quantitative Biology, Peking University, Beijing 100871, China

(Received 31 May 2022; accepted 2 November 2022; published 28 November 2022)

Cellular ATP plays an important role in the calcium oscillation signal transduction pathway of pancreatic β cells. It triggers oscillation by binding the ATP-sensitive K^+ channels (K_{ATP}), and maintains the oscillation by providing ATP hydrolysis free energy for the normal function of ion pumps on the plasma membrane. To reveal how cellular ATP level and ATP hydrolysis free energy affect calcium oscillation, we first constructed a simplified kinetic model of K_{ATP} and calcium pumps, then analyzed their thermodynamic characteristics. Bifurcation of calcium oscillation is determined by both cellular ATP concentration and ATP hydrolysis free energy such that an insufficient ATP energy supply would result in dysfunctional calcium oscillation. Second, to investigate the glucose sensing in β cells, we developed a glycolysis-calcium model that considers the dynamics of ATP and free energy levels. The model simulated three calcium patterns in wild type cells and impaired calcium response of K_{ATP} mutant cells, allowing the use of the ATP-free energy phase plane to explore the underlying mechanism. Our results reveal the thermodynamics of calcium oscillation and provide a framework for understanding the thermodynamics of other ion transport systems.

DOI: 10.1103/PhysRevResearch.4.043142

I. INTRODUCTION

Living cells are molecular open systems; the biochemical steady states and oscillations inside cells are nonequilibrium states far from thermodynamic equilibrium [1,2]. Gibbs free energy of ATP hydrolysis (related to ATP:ADP ratio) is a universal energy source that maintains a cell's state and drives its biological functions [3]. While kinetic studies are only on par with kinematics in mechanics, the notions of energy and force in physical biochemistry are contained in chemical thermodynamics [4].

Calcium oscillation is the core part of pancreatic β cell biology. For example, in the case of glucose-stimulated insulin secretion, intracellular calcium concentration oscillates in response to the intake of glucose, which triggers the exocytosis of insulin secretory granules [5]. It is given that ATP plays a crucial role in this process [6–8]. Cellular ATP level increases through the metabolic degradation of ingested glucose, followed by ATP molecules binding ATP-sensitive K^+ channels (K_{ATP}), thereby depolarizing the membrane electrical potential and triggering calcium oscillations at periods of a few seconds in fast mode. At the same time, calcium pumping on the plasma membrane consumes the free energy from ATP hydrolysis through plasma membrane Ca^{2+} ATPase (PMCA). Apart from such fast Ca^{2+} oscillation, interplay between calcium and metabolism induces ATP fluctuation and different types of calcium patterns in response to varied glucose levels. One typical type of response is a slow mode of calcium oscillation with periods of several minutes, contributing to pulsatile insulin secretion [9].

The phenomenon of calcium oscillation in pancreatic β cells has been the subject of much research. Many mathematical models have taken ATP kinetics into consideration to understand the mechanism of different modes of Ca^{2+} oscillation [7,10,11]. However, a quantitative understanding of the influence of ATP hydrolysis free energy is still lacking in pancreatic β cells. Based on data related to thermodynamics, the ATP:ADP ratio has been observed simultaneously with calcium signals *in vivo* [12,13], and proved to determine the open probability of a K_{ATP} channel [14]. Previous studies hardly included the consumption of ATP hydrolysis in the process whereby PMCA channels pump calcium. Thus, such typical interplay between kinetics and nonequilibrium thermodynamics in pancreatic β cells requires a model that considers both kinetics and thermodynamics of ATP.

*These two authors contributed equally to this work.
†lft@pku.edu.cn

Here, in Secs. II A–II C, we constructed an ATP-constant two-variable thermodynamic model to study the fast oscillation of membrane potential and cellular calcium. Simulations reveal how cellular ATP level (kinetics) and ATP hydrolysis free energy (thermodynamics) affect membrane channels, calcium pumps, and fast Ca^{2+} oscillation in pancreatic β cells. In Sec. II D, since cellular ATP level is associated with ATP:ADP ratio, we further extended the two-variable model by considering glycolysis and dynamics of ATP level and hydrolysis free energy. This model, denoted as the glycolysis-calcium model, can simulate different patterns of slow Ca^{2+} oscillations and the dynamic response of pancreatic β cells to increased glucose levels. We used the ATP-γ (free energy) phase plane to investigate the mechanism of these responses. Moreover, we discussed how K_{ATP} mutation affects glucose sensing in Sec. II E.

II. RESULTS

A. ATP and hydrolysis energy affect membrane channels and calcium pumps

To understand the roles of ATP and hydrolysis free energy in fast Ca^{2+} oscillation, we constructed a thermodynamically valid two-variable model of membrane potential (V) and cytoplasm calcium level ($[Ca^{2+}]$).

Previous mathematical models of Ca^{2+} oscillations in the pancreatic β cell [11,15] involve two separate modules: glycolysis and ion transportation. ATP is an output of the glycolysis module and input of the ion transport part. In our two-variable model, we bypassed the glycolysis step, fixed the ATP level and hydrolysis free energy, and treated them as direct inputs of the calcium oscillation system. We also considered the reversible reactions of ATP hydrolysis in order to reveal its thermodynamic properties. The hydrolysis free energy provided by one molecule of ATP is defined as follows [1,16]:

$$\Delta G_{\mathrm{ATP}} = \Delta G^{0}_{\mathrm{ATP}} + k_B T \ln \frac{[\mathrm{ADP}][\mathrm{Pi}]}{[\mathrm{ATP}]}.$$

For convenience, we introduce the parameter γ to represent the amounts of available free energy for ATP hydrolysis as

$$\gamma = e^{-\Delta G_{\mathrm{ATP}}/(k_B T)} = K_{\mathrm{eq}} \frac{[\mathrm{ATP}]}{[\mathrm{ADP}][\mathrm{Pi}]}. \quad (1)$$

K_{eq} is the equilibrium constant of ATP hydrolysis under standard conditions [16],

$$K_{\mathrm{eq}} = e^{-\Delta G^{0}_{\mathrm{ATP}}/(k_B T)} = 4.9 \times 10^{11}\ \mu\mathrm{M},$$

where $1\ \mu\mathrm{M} = 1\ \mu\mathrm{mol/L} = 10^{-6}$ mol/L. γ determines the direction of the hydrolysis reaction ($\Delta G_{\mathrm{ATP}} = -k_B T \ln \gamma$). When the biochemical reactions are in a thermodynamic equilibrium state, $\gamma = 1$.

Figure 1(a) illustrates the schematic mechanism of fast mode calcium oscillation in pancreatic β cells. First, as a consequence of glucose intake, the ratio of ATP to ADP rises. This closes ATP-sensitive K^+ channels (K_{ATP}) [17] and causes depolarization of the plasma membrane. Depolarization activates the voltage-gated calcium channel and introduces an influx of calcium ions. Because of this influx, calcium pumps transport calcium ions out of the cytosol at a higher rate, restoring calcium concentration in the cytoplasm. This active transport consumes ATP hydrolysis free energy. At high calcium concentration, the calcium-dependent potassium channel (K_{Ca}) will also open and restore outflux of K^+ [18], thus repolarizing the plasma membrane. As both membrane potential and $[Ca^{2+}]$ are restored, a period of calcium oscillation completes. In these processes, membrane potential is affected by ion channels, such as the voltage-dependent calcium channel (VDCC), ATP-sensitive K^+ channel (K_{ATP}), calcium-dependent potassium channel (K_{Ca}), and a ligand-independent potassium channel (K_v). Cy-

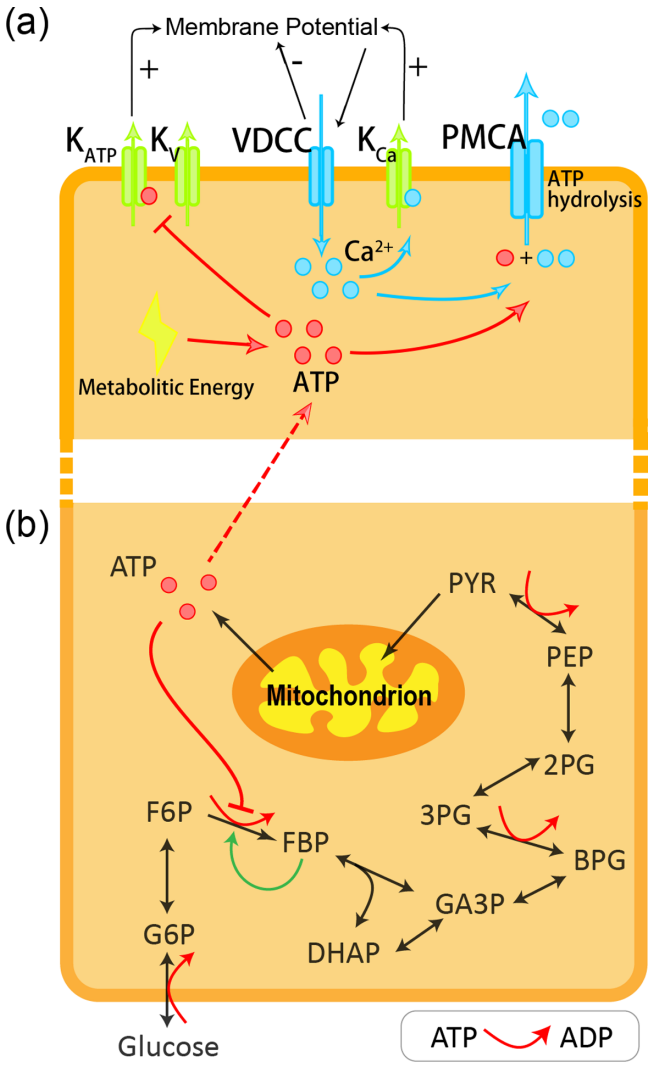

FIG. 1. Schematic calcium oscillation system in pancreatic β cells consisting of membrane ion transport system (a) and glycolysis (b). (a) The ATP-constant two-variable model elucidates the mechanism of fast mode calcium oscillation. Ion channels work together to establish a feedback system involving Ca^{2+}, K^+, and membrane potential. ATP is needed to trigger oscillation through the binding of K_{ATP} and to sustain the oscillation through providing energy for PMCA. (b) Schematic glycolysis combined with ion transport system (a) to build a glycolysis-calcium model and illustrate the mechanism of different calcium oscillation patterns in response to the uptake of glucose. Red curved arrows represent reversible ATP hydrolysis reaction.

toplasm calcium concentration is affected by calcium pumps (PMCA) and VDCC. In addition, the calcium flow through PMCA will not change membrane potential, since each Ca^{2+} ion transports with two H^+ ions crossing the membrane in opposite directions [19].

Based on this fast oscillation mechanism in Fig. 1(a) and previous models [11,15,20], we build an ATP-constant two-variable model of membrane potential V and cytoplasm calcium $[Ca^{2+}]$. The differential equation for V is as follows:

$$\frac{dV}{dt} = -\frac{I_{Ca} + I_K + I_{K(Ca)} + I_{K(ATP)}}{C_m}, \tag{2}$$

where C_m is the membrane capacitance, I_{Ca} indicates calcium ion fluxes through VDCC, I_K indicates potassium ion fluxes through a ligand-independent channel K_v, $I_{K(Ca)}$ indicates fluxes of K^+ through a kind of Ca^{2+}-dependent channel, and $I_{K(ATP)}$ indicates fluxes of K^+ through ATP-sensitive K^+ channels. Among these ion channels, only K_{ATP} interacts with cellular ATP and ADP. We further focus on the roles of cellular ATP concentration ([ATP]) and ATP hydrolysis free energy (γ) in $I_{K(ATP)}$. More details about other ion fluxes can be found in Appendix A 1.

$I_{K(ATP)}$ can be written as

$$I_{K(ATP)} = G_{K(ATP)}\theta(V - V_K),$$

where $G_{K(ATP)}$ is the conductance for the K_{ATP} channel, V_K is the Nernst potential for potassium, and θ is the open probability. The activation conductance adjusts instantaneously to the concentrations of ADP and ATP, but not free energy, and the form of open probability θ is described in detail in Magnus and Keizer (1998a) [21], as Eq. (A8) in Appendix A 1. This formula is built on fitting the experimental data of the open probability of K_{ATP} [17]. Substituting the definition of γ [Eq. (1)], we rewrote the open probability in terms of [ATP] and γ as

$$\theta = \frac{0.08 + 0.026\frac{1}{k_{dd}}\frac{K_{eq}[ATP]}{\gamma[Pi]} + 0.024\left(\frac{1}{k_{dd}}\frac{K_{eq}[ATP]}{\gamma[Pi]}\right)^2}{D_\theta}, \tag{3}$$

where the denominator D_θ is defined as

$$D_\theta = \left(1 + 0.165\frac{1}{k_{dd}}\frac{K_{eq}[ATP]}{\gamma[Pi]}\right)^2 \times \left(1 + 0.135\frac{1}{k_{td}}\frac{K_{eq}[ATP]}{\gamma[Pi]} + 0.05[ATP]/k_{tt}\right).$$

New evidence that ATP hydrolysis results in the formation of this relationship is discussed in Appendix E.

Since only VDCC and PMCA pump calcium, we wrote the equation for $[Ca^{2+}]$ as

$$\frac{d[Ca^{2+}]}{dt} = (-\alpha I_{Ca} - J_{PMCA})f_{cyt}, \tag{4}$$

where α converts current (I_{Ca}) to ion flux, and f_{cyt} is the fraction of free-form Ca^{2+} entering into the cytoplasm. Since only a fraction of Ca^{2+} entering cytoplasm is in free form, we use $f_{cyt} = 0.01$ to denote the ratio [15]. J_{PMCA} is the rate of Ca^{2+} passing through ATPase PMCA, which is the main channel performing active transport of cytoplasmic calcium.

When $[Ca^{2+}]$ rises, PMCA transports calcium ions against concentration gradient into calcium pools, either endoplasmic reticulum (ER) or plasma, by consuming the free energy of ATP hydrolysis. Thus, we further discuss the roles of [ATP] and γ in J_{PMCA}. In our model, we only considered the calcium pool of plasma, and PMCA transports Ca^{2+} through the plasma membrane. Two H^+ ions cross the membrane through ATPases in opposite directions; therefore, as each Ca^{2+} ion is transported [19], membrane potential does not affect the transport of this ion. By considering ATP hydrolysis as a reversible process, the two-variable model becomes thermodynamically valid. Based on Inesi's work [22], we simplify calcium transport through PMCA into a two-step reaction as

$$2Ca^{2+} + E_1 + ATP \underset{k_{-1}}{\overset{k_1}{\rightleftharpoons}} E_2 + ADP,$$

$$E_2 \underset{k_{-2}}{\overset{k_2}{\rightleftharpoons}} 2Ca^{2+}_{pla} + E_1 + Pi.$$

Then the rate of Ca^{2+} passing through PMCA can be written as,

$$J_{PMCA} = 2k_1[Ca^{2+}]^2[E_1][ATP] - 2k_{-1}[E_2][ADP],$$

$$J'_{PMCA} = 2k_2[E_2] - 2k_{-2}[Ca^{2+}]^2_{pla}[E_1][Pi],$$

where J'_{PMCA} is the reaction rate of the second step in PMCA, $[Ca^{2+}]_{pla}$ is free calcium ions in plasma, $[E_1]$ and $[E_2]$ represent the unbinding and binding form of ATPases, respectively, and $[E_1] + [E_2] = [E_T]$ is a constant representing the total amount of ATPases. Thus, we have the kinetic equations for PMCA calcium pumps as

$$\frac{d[E_1]}{dt} = \frac{-J_{PMCA} + J'_{PMCA}}{2},$$

$$\frac{d[E_2]}{dt} = \frac{J_{PMCA} - J'_{PMCA}}{2}.$$

If we adopt a quasisteady assumption, whereby $\frac{d[E_1]}{dt} = \frac{d[E_2]}{dt} = 0$, then the net transportation rate through ATPases can be derived as Eq. (A9). Similarly, J_{PMCA} can be transformed into Eq. (5) in terms of [ATP] and γ as

$$J_{PMCA} = k_{pmca}\frac{k_1k_2[ATP][Ca^{2+}]^2\left(1 - \frac{1}{\gamma}\frac{[Ca^{2+}]^2_{pla}}{[Ca^{2+}]^2}\right)}{D_{PMCA}}, \tag{5}$$

where k_{pmca} replaces $2[E_T]$ for convenience, and the denominator D_{PMCA} is formulated as

$$D_{PMCA} = k_{-1}K_{eq}\frac{[ATP]}{\gamma[Pi]} + k_1[Ca^{2+}]^2[ATP] + k_{-2}[Ca^{2+}]^2_{pla}[Pi] + k_2.$$

Since the calcium pool in plasma is large, we consider $[Ca^{2+}]_{pla}$ as a constant. According to thermodynamic law and nonequilibrium steady state theory [16], an additional relationship holds such that $\frac{k_1k_2}{k_{-1}k_{-2}} = K_{eq}$.

Finally, we obtained a thermodynamically valid and ATP-constant two-variable model to depict the fast mode of calcium oscillation in pancreatic β cells, where Eqs. (2) and (4) depict the cellular membrane potential V and the cytoplasmic concentration of free calcium ions $[Ca^{2+}]$, respectively.

We anticipated that this simplified model would help us reveal the function of Gibbs free energy in the calcium oscillation process.

B. Cellular ATP level and hydrolysis free energy determine calcium oscillation borders

We used the two-variable model to simulate the fast mode of $[Ca^{2+}]$ oscillation and investigate how cellular ATP level and hydrolysis free energy affect such oscillation. Under physiological conditions, $\gamma \approx 10^{10}$, the concentrations for ATP and ADP are 1 and 0.1 mM $= 1 \times 10^{-2}$ mol/L, respectively, while [Pi] is about 1 mM [23]. In our simulation and analysis, we assumed that [Pi] is constant (1 mM); therefore, any two of [ATP], [ADP], and γ were independent variables, and we set them as such. In the simulation, both [ATP] and γ were constants. The other parameters were mostly obtained from published data. We adjusted parameters k_{pmca}, k_1, k_{-1}, k_2 in Eq. (5). More details about the model can be found in Appendix A 1.

Our model successfully generated calcium oscillation. In Fig. 2(a), when [ATP] = 1.4 mM and the free energy is equal to the physical level ($\gamma = 10^{10}$), the period between pulses is 2.22 seconds (27.03 min^{-1}), and the amplitude of calcium oscillation ($[Ca^{2+}]$) is 0.13 μM, which matches fast oscillation in the experiment [24]. Higher [ATP] (= 1.8 mM) speeds up the calcium oscillation with periods ≈1.50 s (40.00 min^{-1}), but maintains the oscillating amplitude, as shown in Fig. 2(a). However, when the concentration of ATP is not high enough, such as [ATP] = 0.9 mM and $\gamma = 10^{10}$, the system does not oscillate. Similarly, γ is responsible for the oscillation. Either [ATP] or γ can determine whether the system is in an oscillatory state. When varying [ATP] or γ, the system can become unstable and start oscillating, which is the point when Hopf bifurcation and saddle node bifurcation of the limit cycle happen (see Appendix B).

In order to quantify the function of ATP level and hydrolysis free energy, we mapped the amplitudes and frequencies of fast $[Ca^{2+}]$ oscillations into the ATP-γ phase plane, as shown in Figs. 2(b) and 2(c). The colored region indicates that oscillation exists in that range of [ATP] and γ, while the region in monochrome dark blue means no oscillation. Transition between stable and oscillating states occurs at the border of the region, i.e., bifurcation. Colors in the oscillating region represent frequency and amplitude in the two subfigures, respectively. We found that the amplitudes remain nearly constant, while the frequencies are much lower near the point of bifurcation.

First, we need to explain the role of [ATP] and γ, respectively. By varying [ATP], the system oscillates within a certain range of [ATP]. Suppose an increase in [ATP] occurs with fixed value of γ. When [ATP] first reaches a certain value, the K_{ATP} channel will be closed, and oscillation will begin, as indicated in Fig. 2. That is a bifurcation. If [ATP] becomes too high, no oscillation occurs because membrane potential cannot be restored under those conditions. It has been observed that oscillation stops when ATP becomes too high [25].

Then, we investigated the role of γ. Under different values of γ, the bifurcation points vary. In the figure, the response of

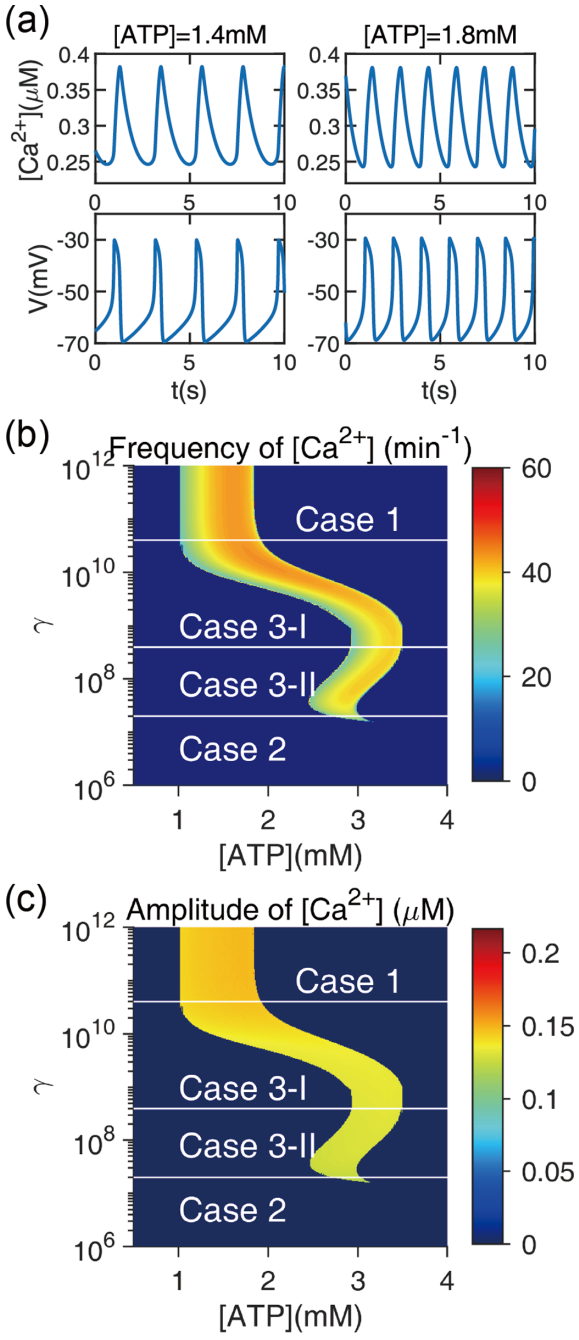

FIG. 2. Cellular ATP level ([ATP]) and hydrolysis free energy (γ) determine fast mode $[Ca^{2+}]$ oscillation. (a) Time courses of fast calcium oscillation under $\gamma = 10^{10}$ and high [ATP] values, the periods (frequencies) of which are 2.22 s. (27.03 min^{-1}) and 1.50 s. (40.00 min^{-1}). (b) The frequencies of calcium oscillations, where the base frequency is extracted from fast Fourier transformation (FFT). (c) The amplitudes of calcium oscillations, defined as the peak-peak values in each stable oscillation. Based on the behavior of bifurcation border, we divide the range of γ into four regions: Case 1, Case 2, Case 3-I, and Case 3-II

bifurcation points to γ can be divided into four regions: Case 1, Case 2, Case 3-I, and Case3-II.

When $\gamma > \gamma_1 \approx 10^{11}$, which is Case 1, γ yields no impact on bifurcation. When γ reaches this high level, the reactions are nearly irreversible. We consider the region of higher γ

to be trivial extrapolation. It should be noted that Case 1 is the region where the reaction of ATPases is approximately irreversible. In our model, this region is above the physiological normal value of $\gamma \approx 10^{10}$ for magnitudes. In fact, under the physiological value of $\gamma \approx 10^{10}$, the reactions of ATPases should not be treated as irreversible.

When $\gamma < \gamma_2 \approx 10^7$, which is Case 2, our model shows that calcium oscillation cannot be generated. This is because PMCA lacks the energy to transport calcium against the chemical gradient. This demonstrates the idea that energy consumption is necessary to maintain the nonequilibrium steady state [16].

The nontrivial result can be seen in both Case 3-I and Case 3-II with $\gamma_2 < \gamma < \gamma_1$, which is where the bifurcation border bends. [ATP] and γ affect bifurcation through the channels of K_{ATP} and PMCA. Here we utilized the nonlinear dynamic method of nullclines on the phase plane to analyze this problem, as shown in Appendix B. We also discuss a four-variable model considering endoplasmic reticulum and a delayed rectifier activation through the K_V channel in Appendix D, and we obtained results similar to those in Fig. 2.

C. Thermodynamic properties of ATP-sensitive K^+ channels and calcium pumps

To understand how thermodynamic properties of ion channels contribute to these cases of calcium oscillation, we investigated the function of [ATP] and γ in K_{ATP} and PMCA.

First, we studied the thermodynamics of K_{ATP} in Figs. 3(a)–3(c), which, indeed, is how [ATP] and γ determine the effect on open probability θ. In Case 3-I and Case 3-II, with $\gamma_2 < \gamma < \gamma_1$, the bifurcation border bends with varying γ. This means bifurcation points are affected by γ. That dependence is a result of enhanced open probability θ [as defined in Eq. (3)] of K_{ATP} within certain range of γ. The relationship between open probability and γ is shown in Fig. 3(a). Around the physiological level of γ ($\gamma \approx 10^{10}$), the open probability of K_{ATP} is largely enhanced. That is further demonstrated in Fig. 3(b), which is the open probability in the parameter space of [ATP] and γ. In this way, high [ATP] level is necessary to close the channel in such a region. In the phase plane, it means that high [ATP] is needed to restore the position of the V nullcline. In fact the $[Ca^{2+}]$ nullcline is hardly affected in Case 3. This leads to the shifts of the bifurcation border.

In our model, PMCA and K_{ATP} channels are the only two that depend on the value of γ. As shown in Fig. 3(c), we investigated the function of K_{ATP} by modifying the PMCA equation such that the system relates to γ only through K_{ATP}. How that is achieved will be explained later. Despite the modification, the bend of the bifurcation border still remains. The high open probability in the bending region requires higher ATP to close the K_{ATP} channel and trigger oscillation. This proves that K_{ATP} is the cause of border bending.

In both Case 3-I, towards higher [ATP], and Case 3-II, towards lower [ATP], the bend of bifurcation borders correlates with the change in K_{ATP} open probability. The function of each case is different. In Case 3-I lower energy would complicate generating oscillation, while in Case 3-II the effect is reversed. It should be noted that Case 3-I is around the physiological level of γ and would be the normal case.

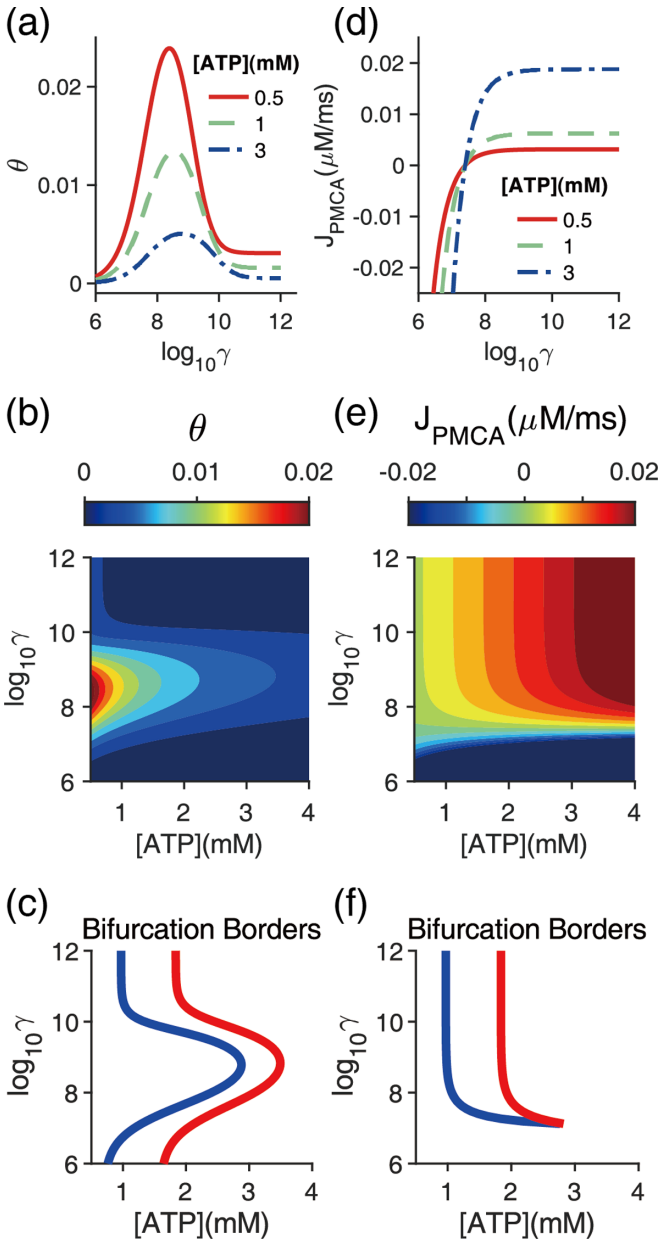

FIG. 3. Thermodynamic analysis of ATP-sensitive K^+ channels (K_{ATP}) and calcium pumps (PMCA). (a) γ affects the open probability θ [in Eq. (3)] of K_{ATP} with different ATP concentrations [ATP]. The open probability would be largely enhanced when $\gamma < \gamma_1 \approx 10^{11}$. (b) The value of θ under different [ATP] and γ. The significant change in $\gamma < \gamma_1 \approx 10^{11}$ leads to the bend of bifurcation border in this region. (c) Bifurcation borders with only K_{ATP} related to γ (PMCA is modified). The bend region of bifurcation borders is consistent with that of original borders in Fig. 2(b). (d) Dependence of J_{PMCA} on γ with various [ATP]. $[Ca^{2+}]$ is fixed at 0.2 μM. At low γ level ($\gamma < \gamma_3 \approx 10^9$), the function of PMCA is significantly affected. The pump would be reversed for $\gamma < 10^7$. (e) J_{PMCA} under different [ATP] and γ. (f) Bifurcation borders with only PMCA related to γ (K_{ATP} is modified). It shows the same cutoff of oscillation region as that in Fig. 2(b), which is under low γ ($\gamma < 10^7$).

We need to demonstrate that the γ region for Case 3 is not just a result of parameter adjustment. The bend of the bifurcation border directly depends on the open probability

θ of K_{ATP}. When the equation of θ is fitted to experimental data [17], it is demonstrated that the change of open probability exists in $\gamma_2 < \gamma < \gamma_1$. Thus, the γ interval where the bifurcation border bends is determined by experimental data. Furthermore, in Appendix C, we analyze the parameter sensitivity numerically to demonstrate that the bend of the border is robust to the change of other parameters. The detailed role of free energy in K_{ATP} is still not clear. The relevant research is ongoing, and ATP hydrolysis is demonstrated to play a role in this process [5]. K_{ATP} has been shown to possess ATPase activity [26]. We discuss the possible molecular mechanism in Appendix E.

Secondly, we further investigated how PMCA consumes free energy to export calcium ions and maintain normal cellular function in calcium oscillation in Figs. 3(d)–3(f). The relationship between the flux through PMCA (J_{PMCA}) and γ is shown in Fig. 3(d). When γ is relatively high, $\gamma > \gamma_3 \approx 10^9$, the reaction of ATPase is nearly irreversible, and J_{PMCA} would saturate to the change of γ. With low γ level ($\gamma < \gamma_3 \approx 10^9$), the function of PMCA is significantly affected by its reversibility, thus it is completely different from the irreversible case. There is a minimal $\gamma_4 \approx 10^7$ under which oscillation would no longer exist.

We derived a theoretical lower boundary of the minimal γ_4 value. The necessary condition is that $J_{PMCA} > 0$, and we can get $\gamma > \frac{[Ca^{2+}]_{pla}^2}{[Ca^{2+}]^2}$. Since the magnitudes of $[Ca^{2+}]_{pla}^2$ and $[Ca^{2+}]^2$ are relatively stable [15,16,24], the lower boundary $\gamma_{lb} \approx 10^7$ is valid. The lower boundary is a good indication of γ_4.

To investigate the function of PMCA, we set the γ-related term in the K_{ATP} equation to be zero ($1/k_{dd} = 1/k_{td} = 0$), and the ATP-sensitive K^+ channel is not affected by γ. However, the dependence of ATPases on γ still remains. The distinctive shape of the bifurcation border is lost [Fig. 3(f)] for the reason explained above, but we still have the cutoff in the low γ region. That is because ATPases do not have sufficient energy to support the oscillation. This is consistent with the result in the activation process of the yeast S phase checkpoint, where a positive feedback loop appears for the phosphorylation of key kinase Rad53 [27].

A PMCA reaction that does not depend on γ is achieved by removing γ-retated terms in Eq. (5). [Pi]-related terms are considered to be unrelated to γ, since we have already assumed [Pi] to be constant in a previous section. In this way, Eq. (5) happens to transform into Michaelis-Menten form, and the reaction is irreversible as follows:

$$J_{PMCA} = \frac{k_{pmca} k_1 k_2 [ATP][Ca^{2+}]^2}{k_1[Ca^{2+}]^2[ATP] + k_{-2}[Ca^{2+}]_{pla}^2[Pi] + k_2}.$$

The bifurcation border at high γ level is similar, but oscillation is not cut off by low γ ($\gamma < 10^7$) in this irreversible case, as shown in Fig. 3(c). This proves the need to consider the reverse reaction, as in the γ-related PMCA in our model. On the phase plane, it can be seen that low γ adds stable fixed points to the limit cycle. Under γ as low as 10^7, the $[Ca]^{2+}$ nullcline shifts dramatically [see Fig. 8(c)]. Two other stable fixed points emerge as the nullclines intersect at an unstable branch. In this way, the system is globally stable.

D. ATP-γ phase plane elucidates the mechanism of Ca^{2+} response to different glucose levels

In response to different levels of glucose absorbed, pancreatic β cells show various $[Ca^{2+}]$ behaviors and insulin secretion rates. To determine the underlying mechanism, we built a glycolysis-calcium model combining the ion transport system and the glycolysis process, as shown in Fig. 1.

Eukaryotic cells, including pancreatic β cells, produce ATP through the processes of glycolysis, the citric acid cycle, and oxidative phosphorylation. Our model focused on the process of glycolysis with a simplified citric acid cycle and oxidative phosphorylation as shown in Fig. 1(b). Using textbook references [28,29], we considered all ten steps of glycolysis: cells absorb glucose (Glu) and phosphorylate it to glucose 6-phosphate (G6P), which is further converted and phosphorylated to fructose1,6-bisphosphate (FBP); the six-carbon sugar phosphate FBP is cleaved into two different three-carbon sugar phosphates, hydroxyacetone phosphate (DHAP) and glyceraldehyde 3-phosphate (GA3P); DHAP is rapidly converted to GA3P, and GA3P ultimately becomes pyruvate (PYR) by five reactions; glycolysis yields two ATP molecules per molecule of glucose. PYR is completely oxidized to CO_2 in the citric acid cycle, the energy of which drives the synthesis of ATP though oxidative phosphorylation in mitochondria.

The glycolysis-calcium model included ten reactants [Eqs. (A10)] and corresponding reactions of glycolysis (v_1 to v_{10} in Table II). The model also includes dynamics of cellular ATP and ADP levels ([ATP] and [ADP]), which are described by

$$\begin{aligned} \frac{d[ATP]}{dt} &= -v_1 - v_3 + v_7 + v_9 + v_{atp} - J_{pmca}^{atp} + v_{ak}, \\ \frac{d[ADP]}{dt} &= -\frac{d[ATP]}{dt} + v_{ak} - 2v_{ak}, \end{aligned} \tag{6}$$

where ATP was consumed by two glycolytic reactions (v_1, v_3), PMCA channels ($J_{PMCA}^{atp} = f_{cyt} J_{PMCA}/2$), and other reactions in the cell, the first term of v_{atp}. We defined v_{atp} when bypassing calcium feedback in the integrated oscillator model [10] as

$$v_{atp} = \frac{1}{\tau_{atp}}\left[-[ATP] + [ADP]\exp\left(1 + \frac{4J_{pyr}}{J_{pyr} + 0.001}\right)\right],$$

where J_{pyr} ($= d_{pyr}[PYR]$) is the degradation and consumption of *pyruvate* (PYR), and τ_{atp} represents the timescale of other phosphorylation reactions in the cell. Meanwhile, ATP production was achieved by two other glycolytic reactions (v_7 and v_9), oxidative phosphorylation (second term of v_{atp}), and the adenylate kinase-related reaction (v_{ak}) as follows:

$$2ADP \underset{k_{ADP}^-}{\overset{k_{ADP}}{\rightleftharpoons}} ATP + AMP.$$

The reaction rate v_{ak} is written as

$$v_{ak} = k_{ADP}[ADP]^2 - \frac{k_{ADP}}{K_{dtm}}[ATP][AMP],$$

where $K_{tdm} = k_{ADP}/k_{ADP}^-$, and cellular AMP concentration [AMP] is calculated by $[AMP] = [A_{tot}] - [ATP] - [ADP]$. The total concentration of adenine nucleotide (A_{tot}) was

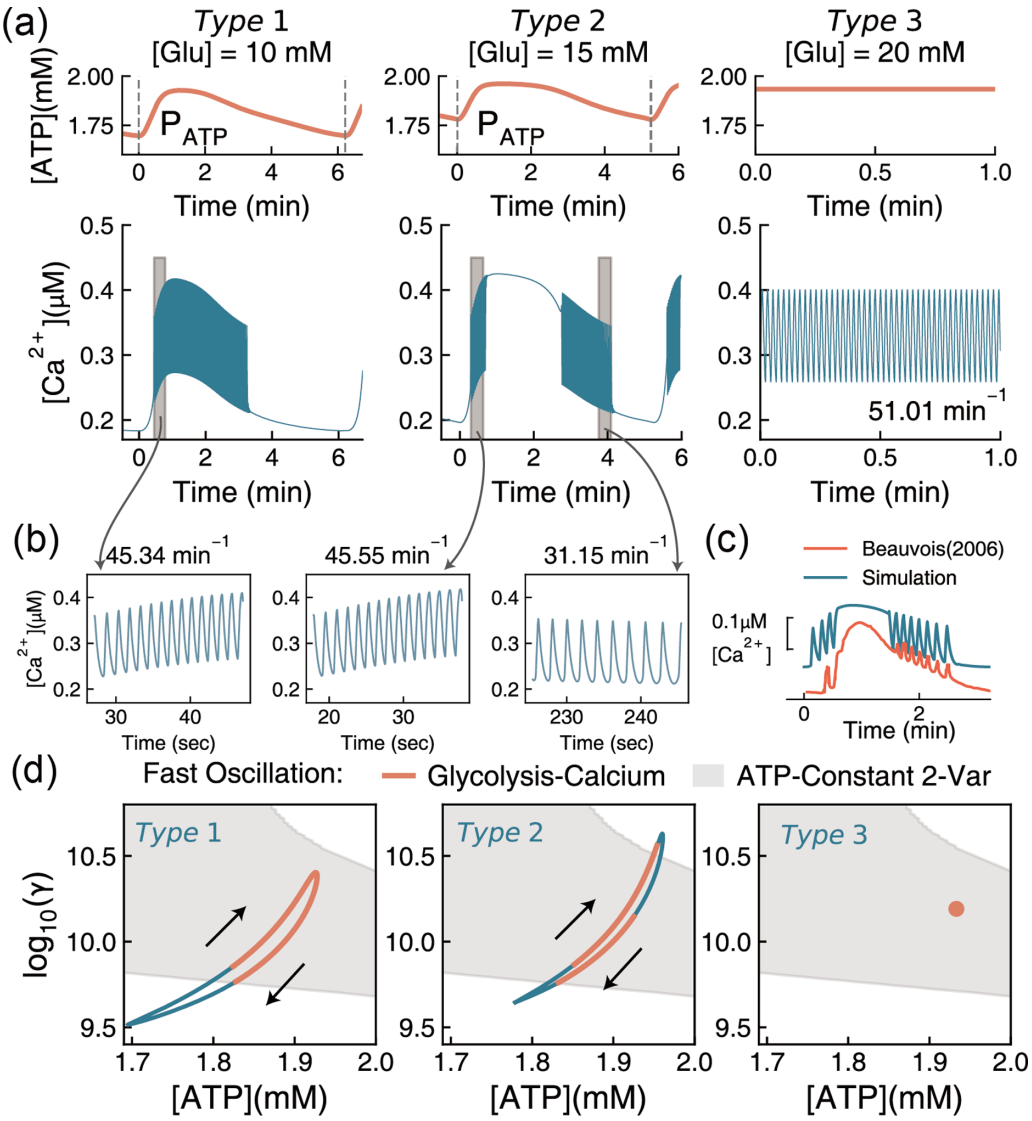

FIG. 4. Different calcium patterns in response to increased glucose concentrations. (a) Examples of three types of $[Ca^{2+}]$ and [ATP] responses to various glucose concentrations, where $[A_{tot}] = 2$ mM. P_{ATP} are the periods of [ATP] oscillation (slow mode), which are 6.23 min for *Type 1* and 5.25 min for *Type 2*. We selected one period of the slow oscillation patterns for *Type 1* and *2*, and defined the oscillation beginning as time zero. (b) The enlarged $[Ca^{2+}]$ patterns of fast mode oscillation in *Type 1* and *2*. Mean periods (frequencies) of three figures are 1.32 s (45.34 min^{-1}, left), 1.32 s (45.55 min^{-1}, middle), and 1.93 s (31.15 min^{-1}, right). (c) Experimental (orange) [9] and model predicted (blue) *Type 2 reversed calcium oscillation* patterns with modified parameters (details in Appendix G). (d) Trajectories of (a) in [ATP]-γ space. The ATP-constant two-variable model indicates that $[Ca^{2+}]$ oscillates in the fast mode when the system stays in the gray area. In the glycolysis-calcium model, the fast mode $[Ca^{2+}]$ oscillation occurs on the orange line (*Type 1* and *Type 2*) or point (*Type 3*).

fixed as 2000 μM. Details of simulations are listed in Appendix A 2.

Therefore, we built a glycolysis-calcium model, including our ATP-constant two-variable model [Eqs. (4) and (2)], the glycolysis process [Eqs. (A10) and Table II], and kinetic processes of ATP and ADP [Eqs. (6)]. When the glucose concentration ([Glu]) increases, β cells are activated with faster rates of glycolysis, oxidative phosphorylation, and ATP production. At the same time, ATP hydrolysis free energy is elevated. Depending on glucose levels, [ATP] and γ show various responses and further trigger different types of calcium oscillation.

Simulation revealed three types of calcium patterns in response to different glucose levels in Figs. 4(a) and 4(b). *Type 1* is *mixed oscillation*: once [Glu] increases, for example, to 10 mM, cellular ATP level and free energy begin oscillating, thereby triggering the slow mode of calcium oscillation with periods $P_{ATP} = 6.23$ min. At the peak of slow mode oscillation, calcium oscillates in the fast mode at the same time. The period (frequency) of fast oscillation changes from 1 to 3 s (20 to 60 min^{-1}) and depends on [ATP] and γ, which is consistent with Fig. 2. High amplitude and fast mode calcium oscillation will activate insulin secretion and eventually reduce blood glucose level. *Type 2* is *reversed mixed oscillation*: with higher [Glu] (= 15 mM), the fast mode calcium oscillation appears

on rising and falling curves of slow mode patterns $P_{\mathrm{ATP}} = 5.25$ min. *Type 3* is *maximum response*: with sufficiently high glucose level (20 mM), cellular ATP stays at a high level. Hence, the calcium concentration oscillates in the fast mode (period 1.18 s, frequency 51.01 min^{-1}), and the cell secretes insulin at the maximum rate. In addition, Figs. 12 and 13 reveal time courses of other variables when the glucose level elevates continuously. When [Glu] is low (1 mM), the cell is inactivated with low levels of [ATP], [Ca^{2+}], and insulin secretion rate.

The ATP-γ phase plane elucidates the mechanism of glucose-induced responses in Fig. 4(d). We combined simulated trajectories of the glycolysis-calcium model with the fast calcium oscillation region from the ATP-constant two-variable model in Fig. 2. Increased [Glu] changes the steady state of cells from a fixed point outside the oscillation region to circulating trajectories (*Types 1* and *2*), and back to a fixed point (*Type 3*) in [ATP]-$\log_{10}(\gamma)$ space. Thus, the slow mode oscillation of calcium appears with the medium [Glu] from 4 to 18 mM in Fig. 14. For *Type 1*, higher [Glu] (=10 mM) elevates the free energy and ATP level to the calcium oscillation area (gray). Then, the fast mode of calcium oscillation begins (orange), continuing until the system goes out of the oscillation area. For *Type 2*, when [Glu] = 15 mM, the trajectory similarly enters the fast oscillation region through the left border. Then, [ATP] and γ reach maximum values and move out of the fast oscillation region through the right border where the fast mode disappears. In addition, after [ATP] decreases and the cell reenters the fast oscillation region, [Ca^{2+}] oscillates in fast mode again. For *Type 3*, both [ATP] and γ stay at high levels, and thus [Ca^{2+}] only oscillates in fast mode, as represented by the orange region in the phase plane. Consequently, mapping the trajectories to [ATP]-γ space with the fast calcium oscillation region from the two-variable model provides a clear understanding of the calcium response mechanism in β cells.

Our simulation uncovered a special type of calcium response, *reversed mixed oscillation* (*Type 2*). It was observed in experiments [9] shown in Fig. 4(c), but rarely discussed in previous studies. The [ATP]-γ phase plane can explain the mechanism of such an oscillation pattern, as the trajectory crosses over the right border of the fast oscillation region shown in Fig. 4(d). Accordingly, moving the trajectory to the right or the top of ATP-γ space may increase the probability of observing reversed mixed calcium oscillation in the experiment. For example, one can elevate the total adenine nucleotide concentration ([A_{tot}]) to transfer the trajectory to the right, which is simulated in Fig. 15(a).

E. Mutations of K_{ATP} channel influence calcium oscillation and glucose sensing

Extensive research has shown that mutations of K_{ATP} channel impair insulin secretion of pancreatic β cells and result in different types of diabetes [30]. Here, we discussed how K_{ATP} mutations shift the calcium oscillation borders in [ATP]-γ space and yet weaken glucose sensing.

In 2008, Tarasov *et al.* found a mutation in ABCC8/SUR1 (Y356C) of the K_{ATP} channel in type 2 diabetes adults [31]. They demonstrated that the Y356C mutant affects ATP binding affinity to K_{ATP} channels and attenuates glucose-induced membrane depolarization and calcium response. In Fig. 5, we fitted the [ATP]-inhibition curves of wild type (WT-2008), heterozygous mutant (hetY356C), and homozygous mutant (homY356C) by K_{ATP} open probability (θ) in our model [Eqs. (3) and (A8)]. θ is formulated as

$$\theta = \frac{0.08\left(1+2\frac{[\mathrm{MgADP}^-]}{k_{dd}}\right)+0.89\left(\frac{[\mathrm{MgADP}^-]}{k_{dd}}\right)^2}{\left(1+\frac{[\mathrm{MgADP}^-]}{k_{dd}}\right)^2\left(1+\frac{[\mathrm{ADP}^{3-}]}{k_{td}}+\frac{[\mathrm{ATP}^{4-}]}{k_{tt}}\right)},$$

where k_{dd} and k_{td} stand for binding affinities of ADP, and k_{tt} represents the ATP binding affinity [21]. Since Tarasov *et al.* only changed ATP concentrations and did not alter ADP concentration, we fitted experimental data with different k_{tt} and fixed other parameters same as before (Table I). The fitting of WT-2008 data gives $k_{tt} = 1.34\ \mu$M. In Figs. 2 and 3, k_{tt} (WT) is 1 μM based on the experiments of Hopkins *et al.* [17]. The slight difference between values of wild type k_{tt} is probably due to different experimental conditions [17,31].

Figure 5(a) shows that the K_{ATP} mutation reduces inhibition of ATP, as the fitted k_{tt} of hetY356C (2.93 μM) and homY356C (4.70 μM) are larger than the estimated k_{tt} of WT-2008 (1.34 μM). Hence, both Y356C mutants can shift the left border of thge Ca^{2+} oscillation region to the upper right of the wild type's in [ATP]-γ space, as shown in Figs. 5(b)

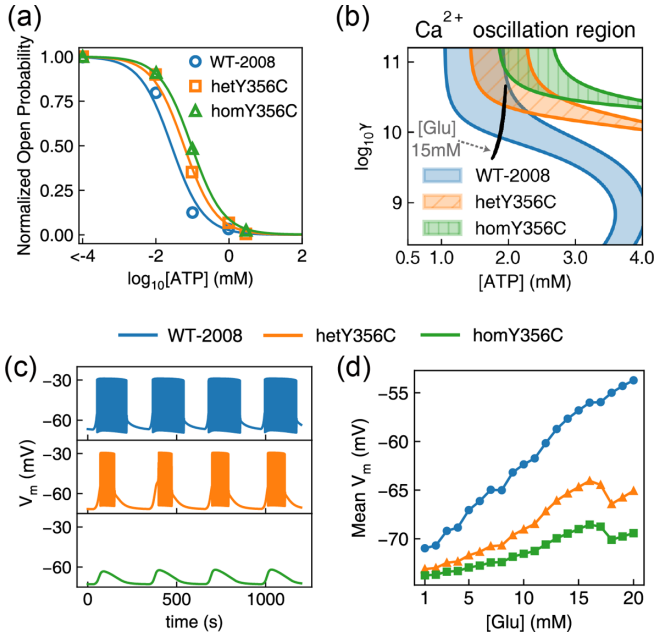

FIG. 5. Comparison between wild type and SUR1-Y356C mutant K_{ATP} channels. (a) Experimental data [31] and fitted ATP-inhibition curves for wild type (WT-2008, blue), heterozygous SUR1-Y356C (hetY356C, orange), and homozygous SUR1-Y356C (homY356C, green). Normalized open probability is calculated by $\theta/\theta_{[\mathrm{ATP}]=0}$ with [ADP] = 0. (b) Fast Ca^{2+} oscillation region in [ATP]-γ space for wild type and mutants of K_{ATP} channels. The black line represents the slow mode oscillation trajectory stimulated by 15 mM glucose. (c) Time courses of membrane potential (V_m) under 15 mM glucose. (d) Pancreatic β cells response to increased glucose levels with or without the SUR1-Y356C mutant. The 20-min averaged V_m quantifies the response level in simulations (points).

TABLE I. Kinetic parameter setting in our ATP-constant model and glycolysis-calcium model. Parameters marked as Ad are the adjusted parameters, the sensitivity analysis of which is discussed in Appendix C. The values of most parameters are adopted from Bertram's model.

Model parameter	Value	Units	Equation in the text	Reference
		Two-variable model		
Pi	1000	μM	(1)	[16]
K_{eq}	4.9×10^{11}	μM	(1)	[16]
k_{pmca}	4	μM	(A9)	Ad
$G_{\text{K(ATP)}}$	25000	pS	$I_{\text{K(ATP)}}$	[15]
$g_{\text{K(Ca)}}$	600	pS	(A6)	[15]
V_{K}	−75	mV	(A6), $I_{\text{K(ATP)}}$, (A3)	[15]
V_{Ca}	25	mV	(A2)	[15]
g_{K}	2700	pS	(A3)	[15]
g_{Ca}	1000	pS	(A2)	[15]
C_m	5300	fF	(2)	[15]
k_D	0.5	μM	(A7)	[15]
k_{dd}	17	μM	(A8)	[21]
k_{td}	26	μM	(A8)	[21]
k_{tt}	1	μM	(A8)	[21]
v_m	−20	mV	(A4)	[15]
v_n	−16	mV	(A4)	[15]
s_m	12	mV	(A4)	[15]
s_n	5	mV	(A4)	[15]
$[Ca^{2+}]_{\text{pla}}$	1000	μM	(A9)	[42]
k_1	1	$\mu M^{-3} ms^{-1}$	(A9)	Ad
k_{-1}	8×10^{-8}	$\mu M^{-1} ms^{-1}$	(A9)	Ad
k_2	5	$\mu M\, ms^{-1}$	(A9)	Ad
α	4.5×10^{-6}	$fA^{-1} \mu M\, ms^{-1}$	(4)	[15]
f_{cyt}	0.01		(4)	[15]
		Glycolysis-calcium model		
$[NAD^+]$	1097	μM	v_6	[43]
[NADH]	1.097	μM	v_6	[43]
$[H^+]$	6.3×10^{-2}	μM	v_6	[43]
k_{pfk}	0.06		J_{pfk}	[10]
K_1	1	μM	W_{ijkl}	Ad
K_2	1	μM	W_{ijkl}	[10]
K_3	5×10^4	μM	W_{ijkl}	[10]
K_4	10^3	μM	W_{ijkl}	[10]
f_{13}	0.02		W_{ijkl}	[10]
f_{23}	0.2		W_{ijkl}	[10]
f_{41}	20		W_{ijkl}	[10]
f_{42}	20		W_{ijkl}	[10]
f_{43}	20		W_{ijkl}	[10]
k_{ADP}	10^{-7}	$\mu M^{-1} ms^{-1}$	v_{ak}	Ad
K_{tdm}	2		v_{ak}	Ad
τ_{atp}	3×10^5	ms	v_{atp}	[10]
d_{pyr}	1×10^{-5}	ms^{-1}	J_{pyr}	Ad

and 6. In Fig. 9(c), we also fitted [ATP]-inhibition curves of other K_{ATP} mutations, while almost 100-fold change of k_{tt} will move fast Ca^{2+} oscillation region outside the space of physiological [ATP] and γ. Besides, we demonstrated that k_{dd} and k_{td}, ADP binding affinities, can also alter the oscillation region but in a different way (Appendix C). Thus, ADP also plays a critical role in K_{ATP} mutation-related diabetes. More experiments are required to investigate how different physiological ADP concentrations affect [ATP]-inhibition curves.

Simulations in Figs. 5(b)–5(d) reveal that the shift of the oscillation region leads to insensitive glucose response. For example, when glucose concentration is 15 mM, most parts of the trajectory lie on the oscillation region for wild type, but few parts or even none of the trajectory cross over the left border for hetY356C or homY356C [Fig. 5(b)]. Under the glucose level that can trigger fast mode oscillation for wild type, K_{ATP} mutant cells have shorter periods or none of fast oscillation response, and hence lower levels of mean membrane potential ($\overline{V_m}$), as shown in Figs. 5(c) and 5(d). Therefore, we demonstrated that mutation induces deficient glucose sensing, which is consistent with experiments [31]. In addition, the steady state of *Type 3* response stays out of the Ca^{2+} oscillation region, leading to the drop of mutant [Glu]-$\overline{V_m}$ curves [Figs. 5(d) and 7].

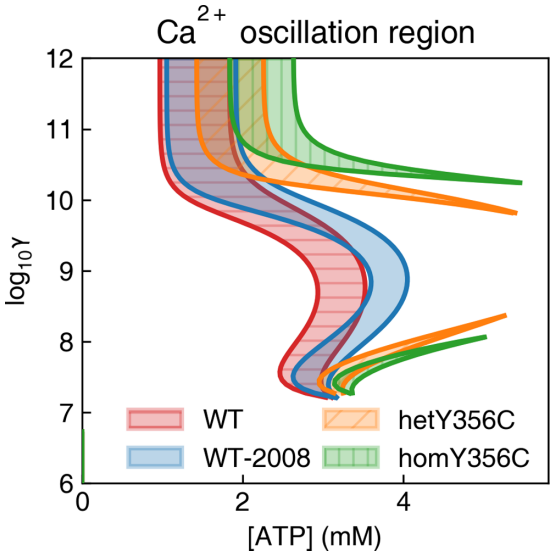

FIG. 6. Calcium oscillation region in wild type and K_{ATP} mutant cells. For WT, we used the parameters in Table I, where $k_{tt} = 1$ μM. Values of k_{tt} for WT-2008, hetY356C and homY356C are estimated as 1.34, 2.93, and 4.70 μM, respectively, while other parameters are same as Table I.

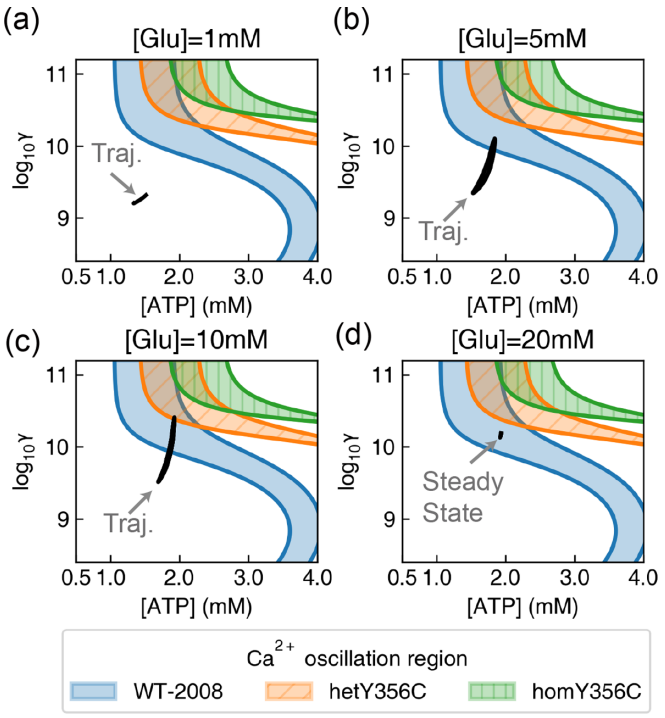

FIG. 7. Different glucose concentrations ([Glu]) stimulate various [ATP]-γ trajectories (Traj.) in wild type or Y356C mutant cells. (a)–(c) Increasing [Glu] leads to the overlap between trajectory and calcium oscillation region in wild type (WT-2008, 5 and 10 mM) and hetY356C mutant cells (10 mM). (d) When [Glu] is high enough (20 mM), the cell reaches a steady state.

III. DISCUSSION

Living cells are thermodynamically open biochemical systems that operate in the nonequilibrium state. While this is widely acknowledged conceptually, we report a quantitative analysis of the interplay between kinetics and thermodynamics of ATP hydrolysis in the sustained calcium oscillations of β cells. In this work, we first constructed a simplified thermodynamically valid two-variable model that contains the reversible reaction of calcium pumps (PMCA) driven by ATP hydrolysis. Consistent with thermodynamic laws, we demonstrated that energy is required for proper function of PMCA. Around the physiological level of the Gibbs free energy, a drop in energy supply would complicate the triggering of calcium oscillation based on the property of the ATP-sensitive K^+ channel (K_{ATP}). Both calcium pumps, which consume energy and sustain oscillation, and the ATP-sensitive K^+ channel determine the dependence of calcium oscillation on ATP hydrolysis free energy ΔG. Second, we built a glycolysis-calcium model to study different types of β-cell responses to increased glucose levels. The ATP-γ phase plane can elucidate the mechanism of these responses, and reveal that a mutant K_{ATP} channel impairs glucose sensing and cellular response of pancreatic β cells.

Our main result is that both cellular ATP and ΔG dominate the bifurcation process of calcium oscillation in β cells. In most cellular physiological environments, ΔG of ATP hydrolysis remains or fluctuates around a basal level. However, under some conditions, it will change distinctly. For example, in aging or abnormal cells, the ability to generate ATP and sustain high ΔG level decreases, which has been observed in aged muscle cells [32]. Meanwhile, the basal level of ΔG can also vary largely in a day. Ohta and coauthors experimentally claimed that ATP:ADP ratios show obvious circadian oscillation in isolated islets of wild type mice during a 12 h light-dark cycle [33]. These changes of basal ΔG level may lead to more complications in calcium oscillation. Our model quantitatively predicts that lower levels of ATP hydrolysis free energy would complicate calcium oscillation. If ΔG is reduced, the bifurcation border would move to the region that needs higher [ATP] level, as in Case 3-I in Fig. 2, or even vanish as in Case 2 in Fig. 2, making it harder to generate oscillation. Some experiments indicate a connection between aging and diabetes [34,35]. It is also possible that a change in other factors, like K_{ATP}, causes, in turn, a shift of the bifurcation border, resulting in similar difficulty.

In Fig. 15, we demonstrate that the adenine nucleotide concentration crucially affects the cellular ATP level, while maintaining the same ΔG. Thus, adjusting adenine nucleotide concentrations is a possible method of modifying cellular ATP levels, while maintaining the thermodynamic state of cells. An ideal experimental system to test the function of ATP hydrolysis free energy should observe calcium oscillation with changing [ATP] and ΔG; however, this is difficult to realize *in vivo* in living cells where mitochondria are continuously producing ATP. Recently, in a simpler *in vitro* system of fission yeast, we experimentally verified the function of ATP and ΔG in the G2-M transition process [36].

A few parts of our model can be explored in the future. For example, other important membrane channels supported by ATP hydrolysis free energy could be discussed. The glycolysis-calcium model currently cannot describe the compound oscillation of calcium, and validity of the PMCA

channel, as well as glycolysis-related parameters, all need additional study in the future. Moreover, a recent study reported that interactions between pancreatic α and β cells contribute to globally phase lock calcium oscillation patterns [37], where the roles of ATP and hydrolysis free energy are still elusive.

To summarize, in this work, we first construct an ATP-constant two-variable model to reveal how ATP hydrolysis free energy determines calcium oscillation in pancreatic β cells. Second, we used a glycolysis-calcium model and ATP-γ phase plane to study the mechanism of β cell response to various glucose concentrations. We showed that cellular ATP and hydrolysis free energy determine the function of ion channels, and thus calcium responses in β cells. As the key method and results in our work, the thermodynamic analysis of ion channels related to ATP-ADP binding and ATP hydrolysis together with the ATP-γ phase plane can be utilized to investigate both kinetic and thermodynamic properties of other ion channels and biological processes.

ACKNOWLEDGMENTS

The authors are grateful to Liangyi Chen, Chao Tang, Lei Chen, Huixia Ren, Chengsheng Han, Yi Yu, and Yibo Bao for helpful discussions. This work was supported by the National Natural Science Foundation of China (Grants No. 12174007 and No. 12090054) and the National Key R&D Program in China (Grants No. 2018YFA0900200 and No. 2020YFA0906900).

F.L. and Q.O. designed the research; D.L., Y.S., C.N., and Y.G. performed model simulations and data analysis; Y.S., D.L., and F.L. contributed to the analytical results; D.L., Y.S., F.L., Q.O., and H.Q. wrote the paper.

The authors declare that no competing interests exist.

APPENDICES

The appendices are arranged as follows: (1) In Appendix A, the details of our models are presented. (2) In Appendices B and C, we perform the bifurcation analysis and the parameter sensitivity analysis of the ATP-constant two-variable model, and simulations predict how different K_{ATP} mutants may affect calcium oscillation borders in [ATP]–free energy space. (3) In Appendices D and E, we prove that our major result in the two-variable model (Fig. 2) is consistent with the results of three detailed calcium-membrane potential models in pancreatic β cells. (4) In Appendices F–J, we list other useful results of the glycolysis-calcium model, including time courses of the variables not presented in the main text (reactants of glycolysis), calcium responses to increasing glucose levels, influence of the total adenine nucleotide (constraining [ATP] maximum), illustration of delays in slow Ca^{2+} oscillation, and the sensitivity analysis of parameters in glycolysis equations.

APPENDIX A: DETAILS OF MATHEMATICAL MODELS

1. ATP-constant two-variable model of membrane potential and cytoplasm calcium concentration

Based on previous models [11,15,20], we proposed an ATP-constant two-variable model of membrane potential V and cytoplasm calcium concentration ($[Ca^{2+}]$) to study fast calcium oscillation in pancreatic β cells,

$$\begin{aligned}\frac{dV}{dt} &= -\frac{I_{Ca}+I_K+I_{K(Ca)}+I_{K(ATP)}}{C_m},\\ \frac{d[Ca^{2+}]}{dt} &= (-\alpha I_{Ca}-J_{PMCA})f_{cyt},\end{aligned} \tag{A1}$$

As $I_{K(ATP)}$ and J_{PMCA} were defined in the main text, other ionic currents are formulated as follows:

$$I_{Ca} = g_{Ca}m_\infty(V)(V-V_{Ca}), \tag{A2}$$

$$I_K = g_K n_\infty(V)(V-V_K), \tag{A3}$$

where g_{Ca} and g_K are conductances for VDCC and K_v, respectively; V_{Ca} and V_K are Nernst potentials for calcium and potassium; $m_\infty(V)$ and $n_\infty(V)$ are their activation factors, adopting rapid equilibrium; v_m and v_n are gate opening voltages.

We incorporated $m_\infty(V)$ directly into I_{Ca} and $n_\infty(V)$ into I_K. The steady state activation functions are as follows:

$$m_\infty(V) = [1+e^{(v_m-V)/s_m}]^{-1}, \tag{A4}$$

$$n_\infty(V) = [1+e^{(v_n-V)/s_n}]^{-1}, \tag{A5}$$

all of which have an increasing dependence on voltage and saturate at large positive voltages.

$I_{K(Ca)}$ indicates fluxes of K^+ through a kind of Ca^{2+}-dependent channel [18], and we have

$$I_{K(Ca)} = g_{K(Ca)}\omega(V-V_K). \tag{A6}$$

The activation factor ω is

$$\omega = \frac{[Ca^{2+}]^2}{[Ca^{2+}]^2+k_D^2}, \tag{A7}$$

where k_D is the dissociation constant for Ca^{2+} binding the channel, and $[Ca^{2+}]$ is the concentration of free calcium ions in cytoplasm.

Before transformed into [ATP] and γ dependent formulas, the original definitions of K_{ATP} channel open probability (θ) and J_{PMCA} are shown in Eqs. (A8) and (A9), where $[MgADP^-] = 0.165[ADP]$, $[ADP^{3-}] = 0.135[ADP]$, and $[ATP^{4-}] = 0.05[ATP]$.

$$\theta = \frac{0.08(1+2[MgADP^-]/k_{dd})+0.89([MgADP^-]/k_{dd})^2}{(1+[MgADP^-]/k_{dd})^2(1+[ADP^{3-}]/k_{td}+[ATP^{4-}]/k_{tt})}, \tag{A8}$$

$$J_{PMCA} = k_{pmca}\frac{k_1k_2[ATP][Ca^{2+}]^2-k_{-1}k_{-2}[ADP][Pi][Ca^{2+}]_{pla}^2}{k_{-1}[ADP]+k_1[Ca^{2+}]^2[ATP]+k_{-2}[Ca^{2+}]_{pla}^2[Pi]+k_2}. \tag{A9}$$

TABLE II. Reactions, equations, and parameters of the glycolysis process in our model.

Reaction[a]	Equation	Positive rate k_i[b]	ΔG_i^0(kJ/mol)[c]
Glucose+ATP↔ ADP+G6P	$v_1 = k_1[\text{Glu}][\text{ATP}] - k_1'[\text{G6P}][\text{ADP}]$	5.0×10^{-11} ($\mu\text{M}^{-1}\text{ms}^{-1}$)	−16.7
G6P ↔ F6P	$v_2 = k_2[\text{G6P}] - k_2'[\text{F6P}]$	2.2×10^{-1} (ms^{-1})	1.7
F6P+ATP→ FBP+ADP	$v_3 = J_{\text{pfk}}$	$5.0 \times 2.5 \times 10^{-2}$ ($\mu\text{M}^{-2}\text{ms}^{-1}$)	−14.2
FBP↔DHAP+GA3P	$v_4 = k_4[\text{FBP}] - k_4'[\text{GA3P}][\text{DHAP}]$	6.7×10^{-2} (ms^{-1})	23.8
DHAP↔GA3P	$v_5 = k_5[\text{DHAP}] - k_5'[\text{GA3P}]$	2.7×10^{-3} (ms^{-1})	7.5
GA3P+Pi+NAD^+ ↔ BPG+NADH+H^+	$v_6 = k_6[\text{GA3P}][\text{Pi}][\text{NAD}^+] - k_6'[\text{BPG}][\text{NADH}][\text{H}^+]$	1.9×10^{-9} ($\mu\text{M}^{-2}\text{ms}^{-1}$)	6.3
BPG+ADP↔3PG+ATP	$v_7 = k_7[\text{BPG}][\text{ADP}] - k_7'[\text{3PG}][\text{ATP}]$	4.8×10^{-4} ($\mu\text{M}^{-1}\text{ms}^{-1}$)	−18.8
3PG↔ 2PG	$v_8 = k_8[\text{3PG}] - k_8'[\text{2PG}]$	7.0×10^{-4} (ms^{-1})	4.4
2PG↔PEP+H_2O	$v_9 = k_9[\text{2PG}] - k_9'[\text{PEP}]$	1.0×10^{-3} (ms^{-1})	7.5
PEP+ADP↔PYR+ATP	$v_{10} = k_{10}[\text{PEP}][\text{ADP}] - k_{10}'[\text{PYR}][\text{ATP}]$	8.8×10^{-5} ($\mu\text{M}^{-1}\text{ms}^{-1}$)	−31.4

[a]G6P: glucose 6-phosphate; F6P: fructose 6-phosphate; FBP: fructose1,6-bisphosphate; DHAP: hydroxyacetone phosphate; GA3P: glyceraldehyde 3-phosphate; BPG: 1,3-bisphosphoglycerate; 3PG: 3-phosphoglycerate; 2PG: 2-phosphoglycerate; PEP: phosphoenolpyruvate; PYR: pyruvate. The dephosphorylation reactions of G6P and FBP are ignored for simplicity.
[b]Parameters were estimated to ensure physiological concentrations of reactants [44] during simulations.
[c]The standard free energy changes were obtained from the textbook [29].

We simulated the fast calcium oscillation mode in pancreatic β cells with our ATP-constant two-variable model. The kinetic parameters are listed in Table I. The time series simulation was performed by the ode15s function of MATLAB.

2. The glycolysis-calcium model

To simulate calcium response to glucose changes, we proposed a glycolysis-calcium model, consisting of our ATP-constant two-variable model [Eqs. (4) and (2)], the glycolysis process [Eqs. (A10), Table II], and kinetic processes of ATP and ADP [Eqs. (6)].

The kinetic equations of glycolysis reactants are written as

$$\begin{aligned}
\frac{d[\text{G6P}]}{dt} &= v_1 - v_2, & \frac{d[\text{F6P}]}{dt} &= v_2 - v_3,\\
\frac{d[\text{FBP}]}{dt} &= v_3 - v_4, & \frac{d[\text{DHAP}]}{dt} &= v_4 - v_5,\\
\frac{d[\text{GA3P}]}{dt} &= v_4 + v_5 - v_6, & \frac{d[\text{BPG}]}{dt} &= v_6 - v_7,\\
\frac{d[\text{3PG}]}{dt} &= v_7 - v_8, & \frac{d[\text{2PG}]}{dt} &= v_8 - v_9,\\
\frac{d[\text{PEP}]}{dt} &= v_9 - v_{10}, & \frac{d[\text{PYR}]}{dt} &= v_{10} - J_{\text{pyr}},
\end{aligned} \tag{A10}$$

where v_i stands for the rate of the ith reaction in glycolysis, and [Glu] represents the glucose concentration. $J_{\text{pyr}} = d_{\text{pyr}}[\text{PYR}]$ and d_{PYR} is the degradation and consumption rate of *pyruvate* (PYR).

To build a thermodynamic model, we assumed all reactions are reversible, except for v_3, and computed their rates by the law of mass action (see details in Table II). The standard free energy ΔG_i^0 defines the value of equilibrium constant $K_{\text{eq}}^{(i)} = \exp[\Delta G_i^0/(RT)] = k_i/k_i'$ for each reaction. We calculated the negative rate constants by the positive ones (k_i) and ΔG_i^0. The reaction v_3 (J_{pfk} : F6P → FBP) was considered as one of the key factors to generate ATP oscillation and slow calcium oscillation, since it involves positive feedback of FBP and negative feedback of ATP [5]. Thus, we accepted the same definition from IOM model [10] for v_3,

$$v_3 = J_{\text{pfk}} = k_3 \frac{W_{1110} + k_{\text{pfk}} \sum W_{ij1l}}{\sum W_{\text{ijkl}}},$$
$$W_{\text{ijkl}} = \frac{\left(\frac{[\text{AMP}]}{K_1}\right)^i \left(\frac{[\text{FBP}]}{K_2}\right)^j \left(\frac{[\text{F6P}]}{K_3}\right)^k \left(\frac{[\text{ATP}]}{K_4}\right)^l}{(f_{13})^{ik}(f_{23})^{jk}(f_{41})^{jl}(f_{43})^{kl}}.$$

All the values of standard parameters in the glycolysis-calcium model can be found in Tables I and II. The initial conditions are $[\text{Ca}^{2+}]_0 = 0.17$ μM, $V_0 = -70$ mV, $[\text{ATP}]_0 = 1800$ μM, $[\text{ADP}]_0 = 150$ μM, $[\text{G6P}]_0 = 200$ μM, $[\text{F6P}]_0 = 100$ μM, $[\text{FBP}]_0 = 25$ μM, $[\text{DHAP}]_0 = 40$ μM, $[\text{GA3P}]_0 = 16$ μM, $[\text{BPG}]_0 = 10$ μM, $[\text{3GP}]_0 = 410$ μM, $[\text{2PG}]_0 = 49$ μM, $[\text{PEP}]_0 = 143$ μM, and $[\text{PYR}]_0 = 187$ μM. We used ordinary-differential-equation solvers in PYTHON 3.8 and MATLAB 2020 to solve the equations with time step equaling 10 ms.

APPENDIX B: BIFURCATION ANALYSIS OF THE ATP-CONSTANT TWO-VARIABLE MODEL

Based on the two-variable model, we investigated and analyzed the fast mode of calcium oscillation in pancreatic β cells on the phase plane of membrane potential V and cytoplasm calcium concentration $[\text{Ca}^{2+}]$. Figures 8(a)–8(c) show the V nullcline ($\frac{dV}{dt} = 0$) and the $[\text{Ca}^{2+}]$ nullcline ($\frac{d[\text{Ca}^{2+}]}{dt} = 0$). The region where the V nullcline folds is a bistable region. The V nullcline has two stable branches (top and bottom) and one unstable branch (middle). At low ATP concentration [Fig. 8(b)], the V nullcline and the $[\text{Ca}^{2+}]$ nullcline intersect at the stable branch. Since the evolve rate of V is often much faster than that of $[\text{Ca}^{2+}]$, the system would first reach the stable state of V under a certain $[\text{Ca}^{2+}]$. After the system approaches the V nullcline, it will then evolve towards the $[\text{Ca}^{2+}]$ nullcline, and finally reach the stable fixed point. With the rise of [ATP], the nullclines move, and intersect at the unstable branch [Fig. 8(a)]. The system cannot reach the fixed point in this case, and it falls off the stable branch into another stable branch. Thus, the system reaches a state of oscillation (limit cycle), whose trajectory is displayed as discrete points with

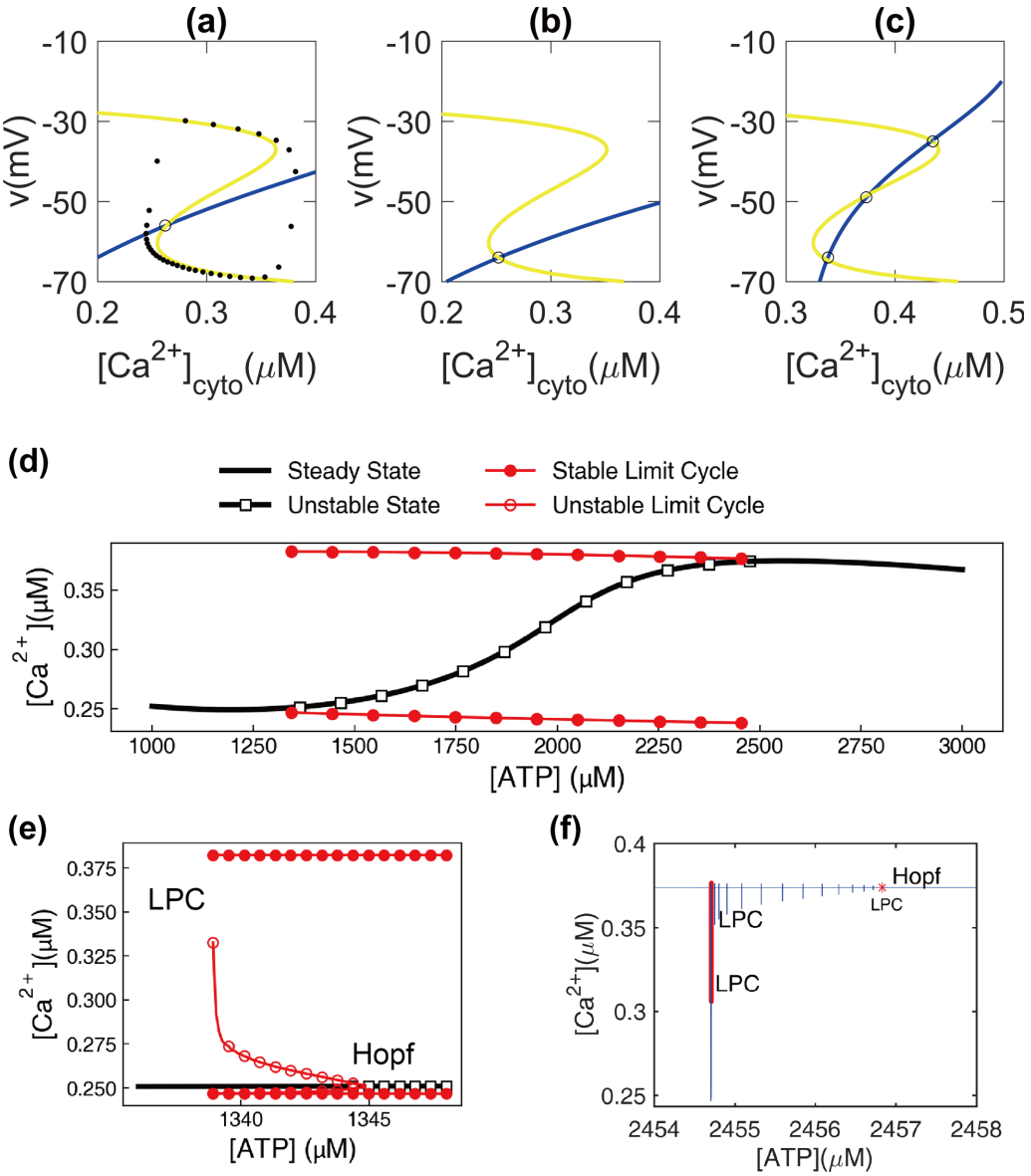

FIG. 8. Bifurcation analysis. (a)–(c) Phase plane of the calcium oscillation system. Blue line: $\frac{d[Ca^{2+}]}{dt} = 0$ nullcline. Yellow line: $\frac{dV}{dt} = 0$ nullcline. Dotted line: stable trajectory of time sequence simulation. Circle: fixed point. (a) Under [ATP] = 1.6 mM and $\gamma = 10^{10}$, the two nullclines yield an unstable fixed point, and a limit cycle emerges. (b) Under [ATP] = 1 mM and $\gamma = 10^{10}$, the decreasing [ATP] makes the fixed point stable, and there is no limit cycle. (c) Under low γ ($\gamma = 10^{7}$) and [ATP] = 4.4 mM, the two nullclines intersect at unstable fixed point, and two additional stable fixed points eliminate the limit cycle. The system is globally stable. (d)–(f) Bifurcation diagram under $\gamma = 10^{10}$. (e) Bifurcation diagram of the left boundary in Fig. 2. (f) Bifurcation diagram of the right boundary in Fig. 2, calculated by MATCONT 7.2. Red lines stand for the limit point bifurcation of cycles (LPC). The red star represents Hopf bifurcation.

equal time interval. Higher density of dots represents lower speed of evolution. Such bifurcation is termed "oscillation caused by hysteresis."

It should be noticed that the fixed point is close to the oscillation trajectory near the bifurcation border. The trajectory gets slowed down near the fixed point since the evolve rates of V and $[Ca^{2+}]$ are lower there. This explains the low frequency near the bifurcation border in Fig. 2. If [ATP] increases further, another bifurcation occurs, and the system would, again, stabilize. This explains the appearance of varying [ATP] results in the two bifurcation branches in Fig. 2. The bifurcation diagram with fixed $\gamma = 10^{10}$ and various [ATP] represents the fixed points and maximum/minimum $[Ca^{2+}]$ of stable limit cycles in Fig. 8(d). The details of bifurcation types at lower (≈1.340 mM) and higher (≈2.455 mM) [ATP] are illustrated in Figs. 8(e) and 8(f). When γ is too low, for example $\gamma = 10^{7}$ in Fig. 8(c), two nullclines always intersect at stable branch, and thus $[Ca^{2+}]$ would not oscillate. We used MATCONT 7.2 in MATLAB to validate our bifurcation diagrams.

APPENDIX C: PARAMETER SENSITIVITY ANALYSIS OF THE ATP-CONSTANT TWO-VARIABLE MODEL AND K_{ATP} CHANNEL

One of our key findings is that the bifurcation border is relatively sensitive to γ in Case 3-I. To exam its robustness

TABLE III. Parameter sensitivity analysis of the bifurcation of [ATP] for the left border. The data involve the percentage difference in bifurcation point values between $\gamma = 10^9$ and $\gamma = 10^{10}$. It is the distance between upper end and bottom end of the border slope. It represents the sensitivity of bifurcation border to γ. In most cases, the distance changes little under a rise or drop of 10% of each parameter. For the parameters V_K and s_m, the changes are considerable since they represent the exponential part of our formula. $G_{K(ATP)}$ exerts significant impact since the sensitivity is determine by the K_{ATP} channel.

	Drop 10%	Raise 10%		Drop 10%	Raise 10%		Drop 10%	Raise 10%
Pi	−2.3%	1.8%	g_{Ca}	8.6%	−7.2%	k_{-2}	0.9%	−1.0%
K_{eq}	2.7%	−3.2%	C_m	0.0%	0.0%	k_1	−1.1%	0.8%
k_{pmca}	−1.3%	1.0%	k_D	−2.2%	1.5%	k_2	−1.1%	0.8%
$[Ca^{2+}]_{pla}$	1.7%	−2.0%	k_{dd}	−3.1%	2.0%	v_m	13.5%	−11.8%
$G_{K(ATP)}$	−8.9%	8.5%	k_{td}	−0.7%	0.6%	v_n	0.0%	0.0%
$g_{K(Ca)}$	2.0%	−2.0%	k_{tt}	−8.2%	7.7%	s_m	36.5%	−20.1%
V_K	−31.0%	48.2%	α	1.1%	−1.1%	s_n	−0.1%	0.1%
V_{Ca}	2.3%	−2.2%	f_{cyt}	0.0%	0.0%			
g_K	0.0%	0.0%	k_{-1}	−0.2%	0.2%			
					normal situation		0.0%	0.0%

against the fluctuation of parameters, we analyzed the relationship between bifurcation points and parameters in our model. We considered the bifurcation point when γ is set to 10^{10} and 10^9, approximately representing the upper end and lower end of the border slope in Case 3-I. The difference between bifurcation points in 10^{10} and 10^9 is calculated and defined as Δ_{ATP}. When $\Delta_{ATP} = 0$, the bend of the border is totally lost. We calculated the percent change of Δ_{ATP} with a shift of each parameter for 10% or −10%. The result is shown in Table III. In most cases, [ATP] only rises or drops about 10% for each parameter. For the parameters V_K, s_m, and v_m, the changes are more significant since they represent the exponential part of our formula and have considerable influence on the result. However, they are also unlikely to change much and, as such, are not the main concern. $G_{K(ATP)}$ and k_{tt} exert significant impact since sensitivity is determined by the K_{ATP} channel. All of the parameters shifts made in this section cannot destroy the bend shape of the border.

To understand how different mutations will affect pancreatic β cells, we discussed the influence of three key parameters (k_{dd}, k_{td}, and k_{tt}) on the open probability θ of K_{ATP} channels in Fig. 9. Increasing k_{dd} results in higher open rates of channels, while larger k_{td} and k_{tt} can inhibit the channel [Fig. 9(a)]. In addition, k_{tt} plays the most critical role in K_{ATP} inhibition, since it can dramatically change the open rate in comparison with other two parameters. Such huge impact of k_{tt} leads to a significant shift of Ca^{2+} oscillation borders, and stops the fast mode oscillation under physiological energy level ($\gamma = 10^{10}$), as shown in Fig. 9(b). Increasing k_{dd} may retrieve the ability of glucose sensing and calcium response, as its bifurcation (oscillation) borders shift to the bottom left of the wild type's. For k_{td} perturbation, only borders around high [ADP] (low γ) shift, while borders of physiological level remain unaffected. To further study mechanism of various mutations, we proposed a 24-states model of K_{ATP} channels in Appendix E.

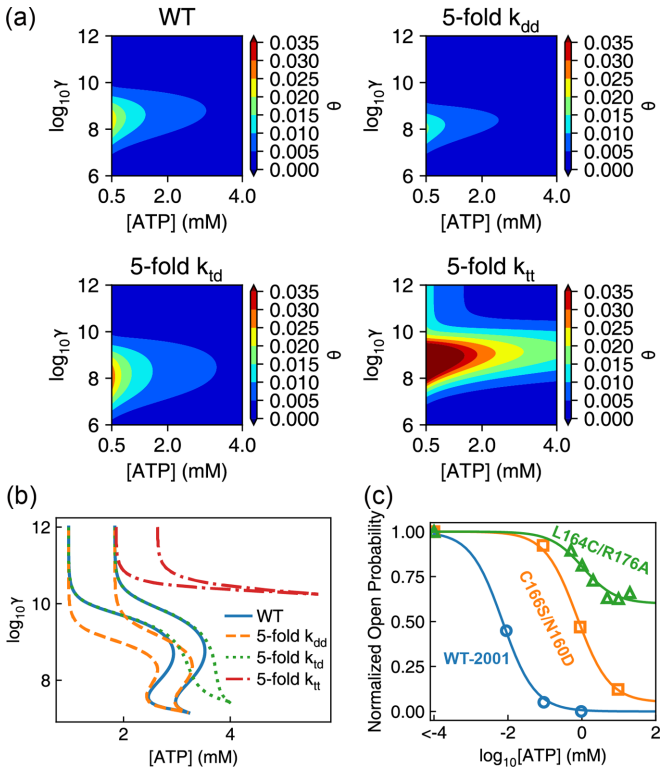

FIG. 9. Influence of three key parameters in K_{ATP} channels. (a) Open probability (θ) for wild type (Table I), fivefold k_{dd}, fivefold k_{td}, or fivefold k_{tt}. (b) Bifurcation borders of the fast Ca^{2+} oscillation region for wild type or parameter perturbation conditions. (c) Experimental points [38] and fitted ATP-inhibition curves for wild type (WT-2001, blue) and two mutants: C166S/N160D (orange) and L164C/R176A (green). Normalized open probability is calculated by $(\theta + \theta_0)/\theta_{[ATP]=0}$ with [ADP] = 0. Fitted k_{tt} of wild type (0.36 μM) is much smaller than k_{tt} of mutants: 37.1 μM for C166S and 53.1 μM for L164C. Mutant L164C shows a basal open rate ($\theta_0 = 0.119$) when [ATP] = 0.

APPENDIX D: THE ATP-CONSTANT FOUR-VARIABLE MODEL OF FAST CALCIUM OSCILLATION IN PANCREATIC β CELLS

We investigated a more complicated model with four variables for calcium oscillation in pancreatic β cells, in which we consider the endoplasmic reticulum (ER) as another calcium pool, and delayed rectifier activation through the K_V channel.

To incorporate ER, the model includes the sarcoendoplasmic reticulum (SR) calcium transport ATPase (SERCA), a Ca^{2+} ATPase that transfers Ca^{2+} from the cytosol to the lumen of SR at the expense of ATP hydrolysis. SERCA function is in a manner similar to that of PMCA:

$$J_{\mathrm{SERCA}} = k_{\mathrm{serca}}\{k_1k_2[\mathrm{ATP}][\mathrm{Ca}^{2+}]^2 - k_{-1}k_{-2}[\mathrm{ADP}][\mathrm{Pi}][\mathrm{Ca}^{2+}]_{\mathrm{er}}^2\}/D_{\mathrm{SERCA}}, \quad \text{(D1)}$$

$$D_{\mathrm{SERCA}} = k_{-1}[\mathrm{ADP}] + k_1[\mathrm{Ca}^{2+}]^2[\mathrm{ATP}] + k_{-2}[\mathrm{Ca}^{2+}]_{\mathrm{er}}^2[\mathrm{Pi}] + k_2, \quad \text{(D2)}$$

where $[Ca^{2+}]_{er}$ is the concentration of calcium in ER, and SERCA calcium ATPases also consume ATP for transportation.

A leaking rate of calcium is responsible for getting calcium out of ER lumen. The function for leaking is

$$J_{\mathrm{leak}} = P_{\mathrm{leak}}([\mathrm{Ca}^{2+}] - [\mathrm{Ca}^{2+}]_{\mathrm{er}}). \quad \text{(D3)}$$

Delayed rectifier activation changes the expression of the activation factor for voltage-dependent potassium channels (n) into

$$\frac{dn}{dt} = [n_\infty(V) - n]/\tau_n, \quad \text{(D4)}$$

$$n_\infty(V) = [1 + e^{(v_n - V)/s_n}]^{-1}. \quad \text{(D5)}$$

Incorporating these two indices, the model becomes a modified thermodynamically valid version of the model by Bertram *et al.* [15]. Thus, we built a ATP-constant four-variable model, formulated as

$$\frac{dV}{dt} = -[I_{\mathrm{Ca}} + I_{\mathrm{K}} + I_{\mathrm{K(Ca)}} + I_{\mathrm{K(ATP)}}]/C_m, \quad \text{(D6)}$$

$$\frac{dn}{dt} = [n_\infty(V) - n]/\tau_n, \quad \text{(D7)}$$

$$\frac{d[\mathrm{Ca}^{2+}]}{dt} = f_{\mathrm{cyt}}(J_{\mathrm{leak}} - J_{\mathrm{SERCA}} - \alpha I_{\mathrm{Ca}} - J_{\mathrm{PMCA}}), \quad \text{(D8)}$$

$$\frac{d[\mathrm{Ca}^{2+}]_{\mathrm{er}}}{dt} = f_{\mathrm{er}}R_{\mathrm{ce}}(-J_{\mathrm{leak}} + J_{\mathrm{SERCA}}), \quad \text{(D9)}$$

where R_{ce} is the volume ratio of cytosol and ER; f_{cyt} and f_{er} are the fractions of free calcium ions to total Ca^{2+} in cytosol and ER respectively.

We simulated the function of ATP hydrolysis in this complicated model, shown in Fig. 10. The results agree largely with the result of the simplified two-variable model in Fig. 2, especially for the S-shape borders of the oscillation region in [ATP]-γ space. The difference between four- and two-variable model is that $[Ca^{2+}]$ oscillation in the four-variable model can occur in the northeast region where the two-variable model only has a steady $[Ca^{2+}]$. However, as shown in Fig. 10(b), oscillations in this region exhibit too high frequency, larger than 108 min^{-1}, and too low amplitude, smaller than 0.02 μM. Such oscillations cannot be considered as the physiologically effective ones. Hence, the four-variable model exhibits an S-shape oscillation region similar to that of the two-variable model in [ATP]-γ space.

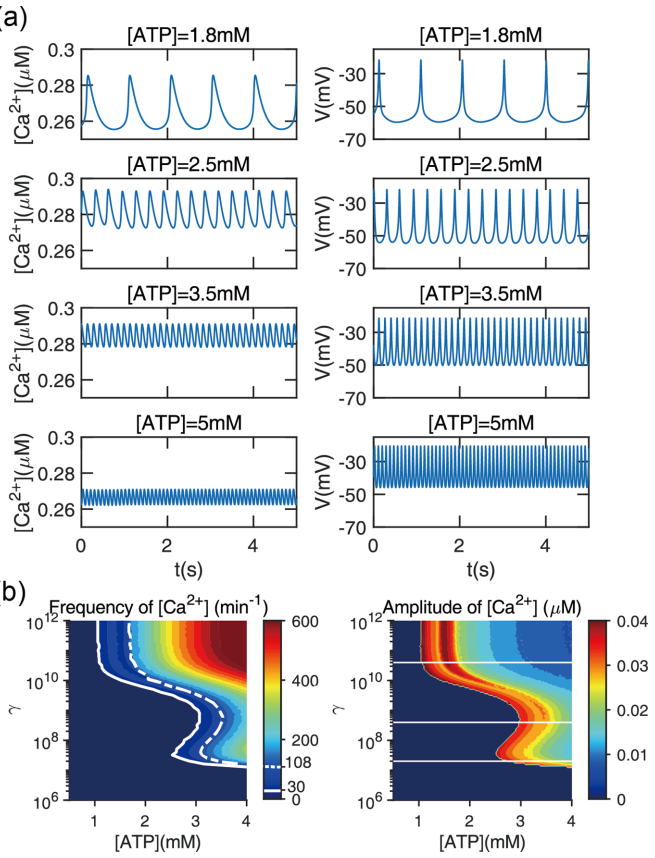

FIG. 10. Results of the ATP-constant four-variable model. (a) Time courses under $\gamma = 10^{10}$ and different ATP levels. (b) Phase maps of calcium oscillation frequency and amplitude. (left) The white solid and dashed curves represent the contour lines where frequencies are 30 and 108 min^{-1}, respectively. (right) The horizontal white lines are the borders of four cases defined in Fig. 2(b) and 2(c).

APPENDIX E: MODELS OF ATP-SENSITIVE K^+ CHANNEL

In this section, we built two alternative models for the ATP-sensitive potassium Channel (K_{ATP}) to illustrate the origin of the unique dependence of K_{ATP} on ATP and its hydrolysis free energy.

K_{ATP} consists of two submodules, Kir 6.2 and SUR1. ANP (ATP or ADP) can bind Kir 6.2 and close the channel, while MgANP (MgATP or MgADP) binding domains on SUR1 opens the channel. In the first model based on the mechanism brought up by Vedovato *et al.* [39], the binding and unbinding states of Kir 6.2 and SUR1, together with the open and closed states of the pore itself, are integrated into an 18-state model. We simulated the channel when ATP and ADP

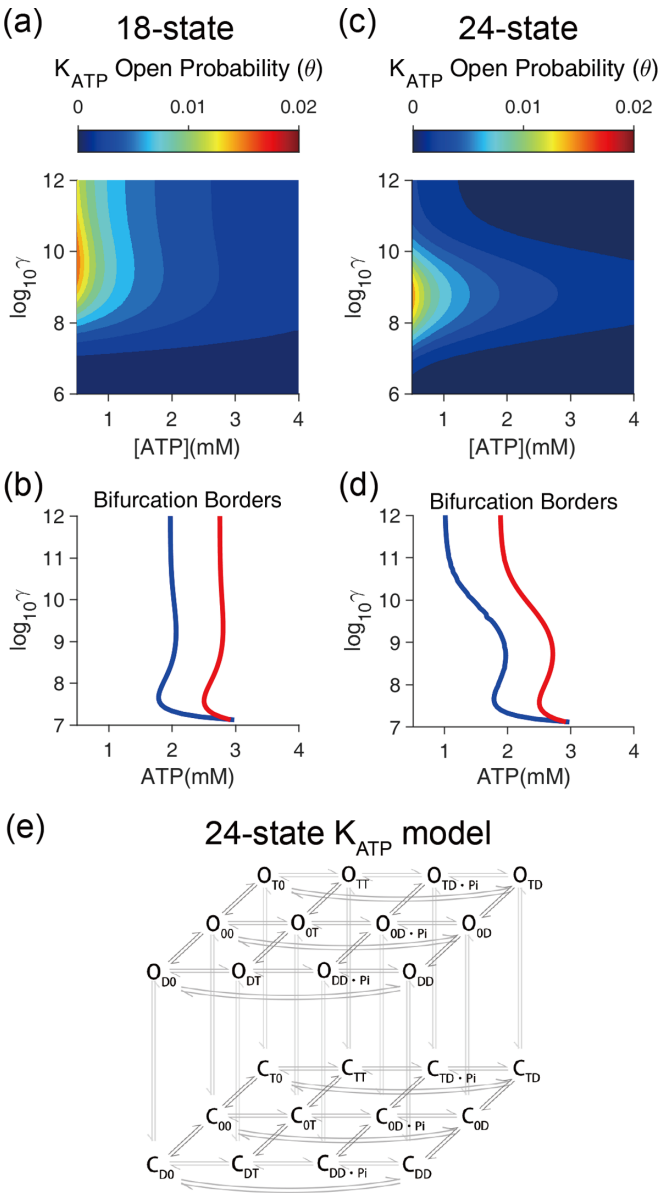

FIG. 11. Comparison between two K_{ATP} models. (a)–(b) Results of the detailed balanced 18-state K_{ATP} model developed from Vedovato *et al.* [39]. (a) Opening probability of the K_{ATP} channel from the detailed balanced model. The channel is in an environment where both ATP and ADP exist. (b) Bifurcation borders after incorporating the detailed balanced model. (c)–(e) Results of our 24-state K_{ATP} model. (c) Opening probability of the K_{ATP} channel. (d) Bifurcation borders. The sensitivity of borders can be retained, but the parameters have not been tested by existing data. (e) Illustration of the K_{ATP} model after considering thermodynamic laws. It has 24 states. C and O are the close and open states of the pore. The first and second subscripts are the ATP and ADP binding states of Kir 6.2 and SUR1, respectively. 0 means unbound, D and T stand for bound with ADP or ATP. D · Pi means hydrolyzed ATP with ADP and Pi, both bound on the SUR1 binding site. The equilibrium constant of ATP hydrolysis has exerted restrictions on the parameters. Detailed balance cannot exist in this model.

are both present. In that case, the opening probability (θ) and bifurcation borders integrating the PMCA channels effect are shown in Figs. 11(a) and 11(b). It can be seen that the bifurcation border is not sensitive to free energy variation, especially in $10^9 < \gamma < 10^{12}$. The above model has the advantage of integrating more details of the molecular mechanism. The disadvantage, however, is its invalidity when thermodynamic properties are considered. The model assumes that the channel reaches an equilibrium, and hence no energy consumption is coupled to the reaction. Nevertheless, the MgANP binding site on SUR1 hydrolyzes MgATP [39], which would consume ATP hydrolysis free energy.

Then, we built another thermodynamically valid model with 24 states. All of the reactions are reversible, and reaction rates are constrained by the equilibrium constant of ATP hydrolysis. The model is shown in Fig. 11(e). The opening probability (θ) and bifurcation borders integrating the PMCA channels effect are shown in Fig. 11(c) and 11(d), respectively. With this modification, it can be seen that sensitivity to free energy (γ) is retained, which matches our result in Fig. 3(b) of the main text. However, this model has too many parameters, and it is overfitted.

APPENDIX F: MODELING THE GLYCOLYSIS-DRIVEN CALCIUM OSCILLATION IN RESPONSE TO VARIOUS GLUCOSE CONCENTRATIONS

We simulated the β-cell response to stepped up growth of glucose concentrations, which is a common experiment paradigm. In Figs. 12 and 13, increased glucose concentrations stimulated glycolysis-driven slow mode oscillation (*Type 1*), reversed mixed oscillation (*Type 2*), and finally induced calcium oscillation of fast mode (*Type 3*). When glucose level was saturated (20 mM), the amplitude of ATP oscillation was reduced, while the ATP level reached a plateau.

APPENDIX G: CALCIUM PATTERNS IN RESPONSE TO GLUCOSE LEVELS, AND REVERSED CALCIUM OSCILLATION PATTERNS IN EXPERIMENTS

The glycolysis-calcium model predicted *Type 2 reversed mix pattern* of $[Ca^{2+}]$, which is observed in the experiments [9] in Fig. 4(c). In simulation, we took the same glucose level in experiments ([Glu] = 8 mM), while modifying three parameters, $[A_{tot}] = 2.7$ mM, $k_3 = 6 \times 10^{-2}$ $\mu M^{-2} ms^{-1}$, and $d_{pyr} = 10^{-4}$ ms^{-1}. We fixed other parameters as shown in the Table I. Periods of fast and slow mode oscillations are 8.33 s and 3.23 min, respectively.

In Fig. 14, we investigated how calcium responds to the glucose level ranging from 1 to 25 mM, with 2 mM $[A_{tot}]$. When [Glu] increases, calcium patterns change from no fast oscillation or steady state ("None") to *Type 1*, *Type 2*, and *Type 3* oscillation patterns. During the process, mean $[Ca^{2+}]$ elevates, and may cause higher speed of insulin secretion, although the curve of mean $[Ca^{2+}]$ is strange in the *Type 2* region. Mean $[Ca^{2+}]$ is the time average $[Ca^{2+}]$ among one period of [ATP] oscillation (P_{ATP}) for *Type 1* and *2*, and 30 minutes for "None" and *Type 3*

APPENDIX H: INFLUENCE OF THE TOTAL ADENINE NUCLEOTIDE ON CALCIUM RESPONSES

We further used the ATP-γ phase plane to study how concentrations of glucose and total adenine nucleotide ($[A_{tot}]$)

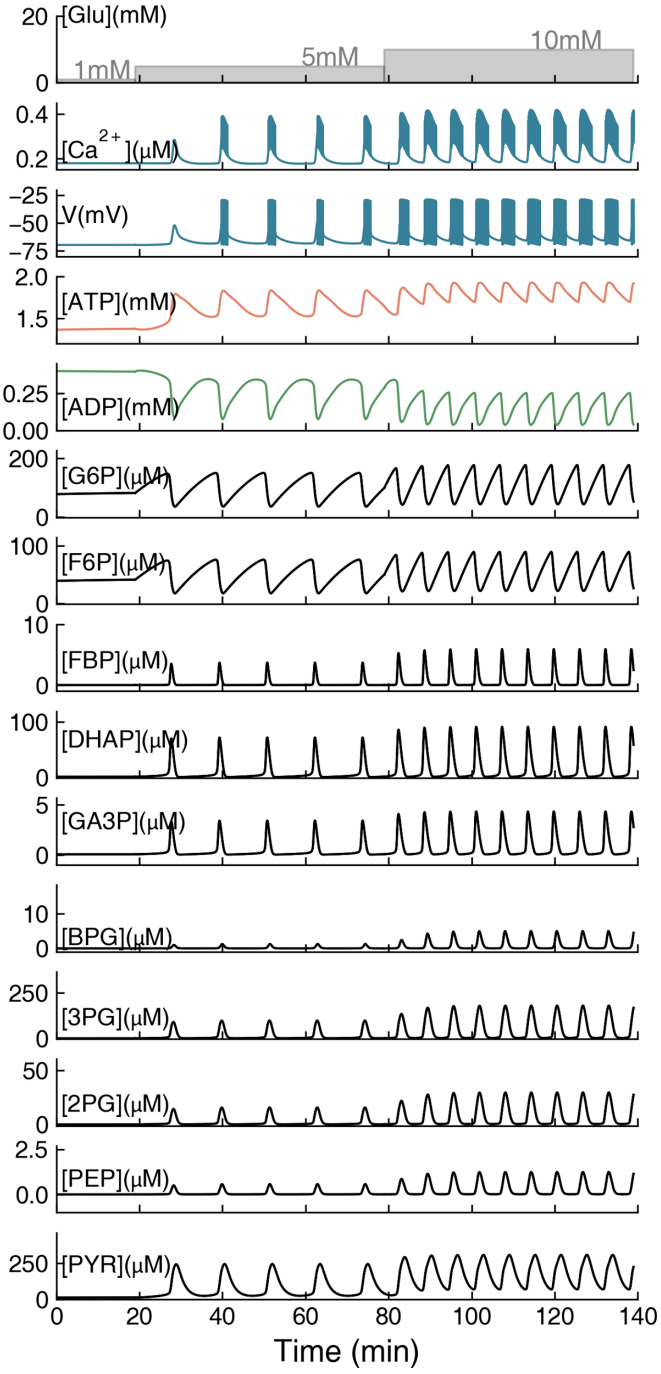

FIG. 12. Schematic of increasing glucose concentrations (from 1 to 10 mM) affecting cellular levels of cytoplasm calcium, ATP, ADP and all glycolysis reactants, calculated by the glycolysis-calcium model with $[A_{\text{tot}}] = 2$ mM. Top gray lines are the glucose concentrations, [Glu].

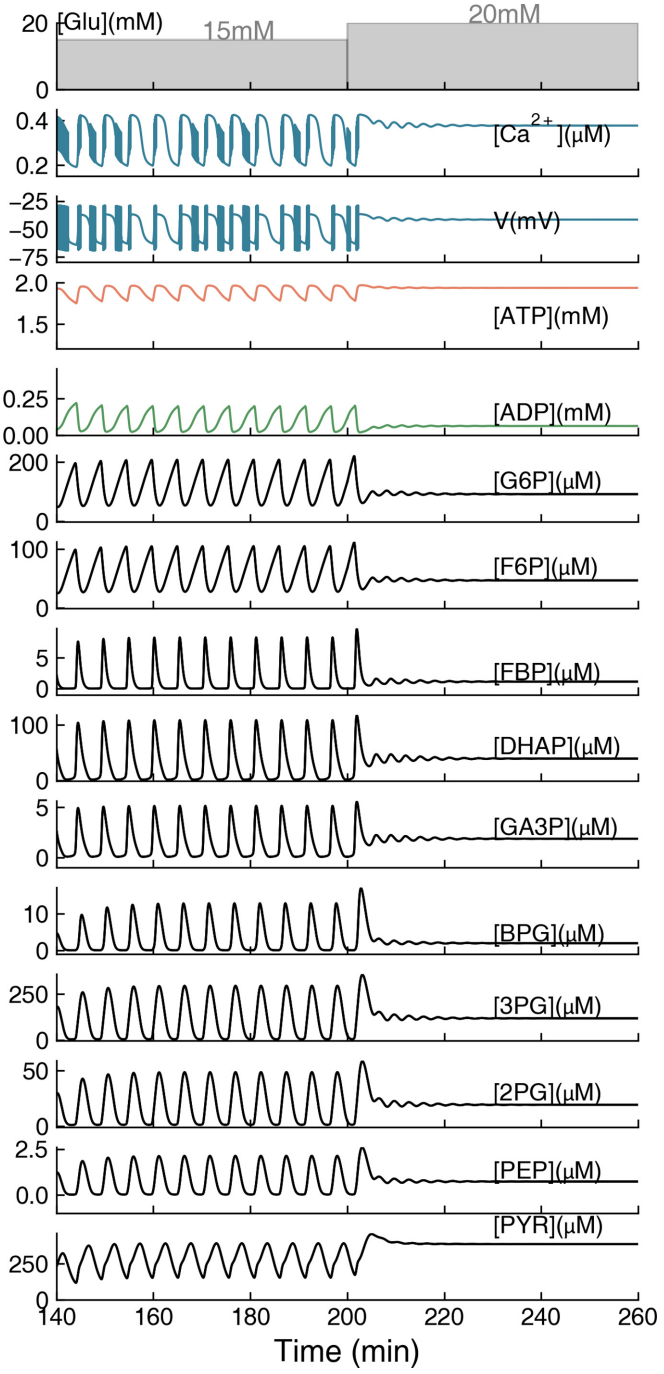

FIG. 13. Schematic of increasing glucose concentrations (from 15 to 20 mM) affecting cellular levels of cytoplasm calcium, ATP, ADP, and all glycolysis reactants, calculated by glycolysis-calcium model with $[A_{\text{tot}}] = 2$ mM. Top gray lines are the glucose concentrations, [Glu].

affect cell responses. We supposed that the insulin secretion rate is positively related to average calcium levels in β cells. Thus, we defined the mean calcium concentration ($\langle \text{Ca} \rangle_t$) as

$$\langle \text{Ca} \rangle_t = \frac{\int_0^{P_{\text{ATP}}} [\text{Ca}^{2+}](\tau) d\tau}{P_{\text{ATP}}}.$$

The score function $\langle \text{Ca} \rangle_{\text{norm}}$ is the normalized $\langle \text{Ca} \rangle_t$, and represents the relative insulin secretion rate,

$$\langle \text{Ca} \rangle_{\text{norm}} = \begin{cases} 0, & \text{no fast oscillation,} \\ \dfrac{\langle \text{Ca} \rangle_t - c_{\min}}{c_{\max} - c_{\min}}, & \textit{Types 1 and 2,} \\ 1, & \textit{Type3,} \end{cases}$$

where the minimum $\langle \text{Ca} \rangle_t$, $c_{\min}$, is 0.179 μM, and the maximum one $c_{max} = 0.341$ μM with $[A_{\text{tot}}] = 2$ mM.

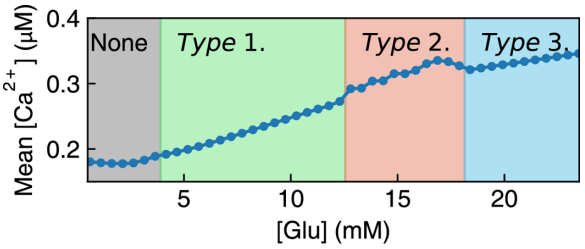

FIG. 14. Different glucose concentrations induce three types of calcium responses under $[A_{tot}] = 2$ mM, while low glucose level cannot activate the cell ("None"). Lower [Glu] thresholds are 4.2 mM (*Type 1*), 12.8 mM (*Type 2*), and 18.4 mM (*Type 3*).

In Fig. 15(b), the response $\langle Ca \rangle_{norm}$ increases linearly with higher glucose concentrations, when $G_0 \leqslant [Glu] \leqslant G_1$. The higher [Glu] indeed enlarges the overlap between trajectory and fast calcium oscillation area. Meanwhile, decreased total concentration of adenine nucleotide ($[A_{tot}]$) weakens the response to the same [Glu]. The reason is that decreasing $[A_{tot}]$ indeed reduces the ATP level while maintaining the free energy of cell, which moves the ATP trajectory out of the fast calcium region, shown in Fig. 15(a). Recent studies have reported the dramatic reduction of total adenine nucleotide concentrations in atrophic skeletal muscle cells

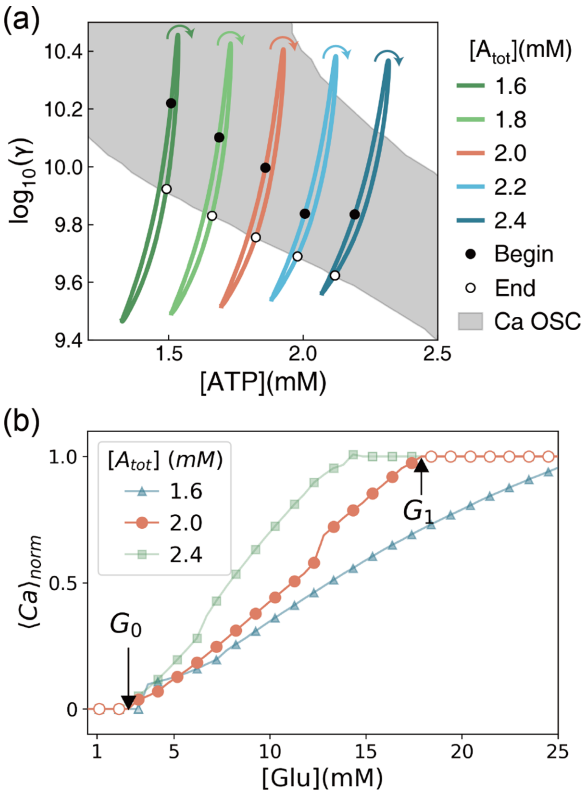

FIG. 15. Concentration of adenine nucleotide ($[A_{tot}]$) affects the metabolism-driven calcium oscillation. (a) ATP trajectories with different $[A_{tot}]$ in [ATP]- $\log_{10}(\gamma)$ space, where [Glu] = 10 mM. (b) Relations between the score function of Ca^{2+} responses and glucose concentration with various $[A_{tot}]$. $G_0 = 2.64$ mM and $G_1 = 17.89$ mM.

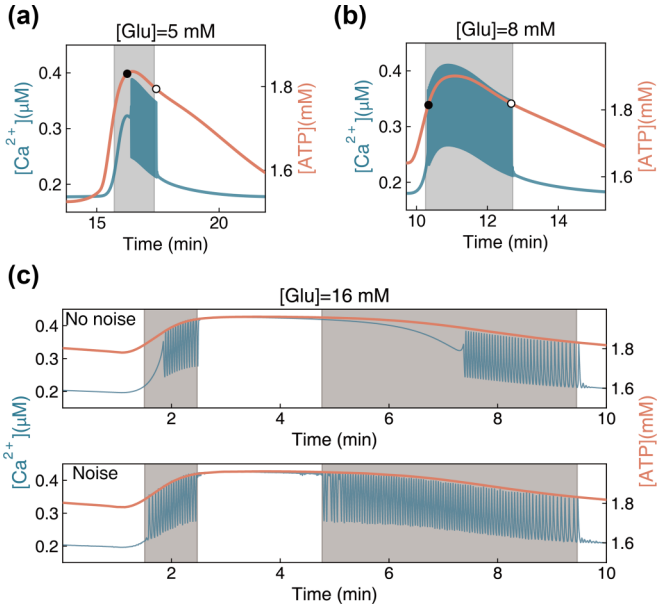

FIG. 16. Delayed calcium oscillation patterns with or without noise. (a)–(b) The length of delayed time is reduced by increasing glucose concentrations. The black and white points stand for the specific values of [ATP] and γ where the fast calcium oscillation begins and ends, respectively. (c) Time courses of calcium and ATP concentrations with (bottom) or without (top) noise. (a)–(c) The gray area represents the ATP range of fast calcium oscillation computed by the ATP-constant two-variable model. $[A_{tot}] = 2$ mM.

in many disease- or aging-associated atrophy [32,40]. Thus, $[A_{tot}]$ is possibly one of the key factor that affects the insulin response of β cells.

APPENDIX I: DELAYED FAST MODE OSCILLATION, AND THE INFLUENCE OF ADENYLATE KINASE IN THE GLYCOLYSIS-CALCIUM MODEL

For *Type 1* or *2* response, when the cell state enters the fast calcium zone (gray) through left or right boarder, the calcium needs a certain delayed time to begin fast oscillation, shown in Figs. 16(a) and 16(c). Generally, cellular reaction rates continuously fluctuate due to internal or external noise. When the noise is considered in the model, fast oscillation immediately begins when the cell enters the region without any delay. In Fig. 16(c), the fast oscillation ranges on the rising and falling curves of the *Type 2* $[Ca^{2+}]$ pattern are consistent with the ATP-constant model prediction (stochastic simulation details are shown as below). Specifically, for *Type 1*, the delayed time is reduced with higher [Glu]; see Figs. 16(a) and 16(b). When the ATP trajectory move out of the fast zone, the fast oscillation directly disappears in both patterns. Thus the fast mode region of the ATP-constant model is a reliable analysis tool for β-cell responses.

To reveal the influence of reaction noise, we a built stochastic glycolysis-calcium model based on chemical Langevin equations [41]. x_i is one of the variables in the glycolysis

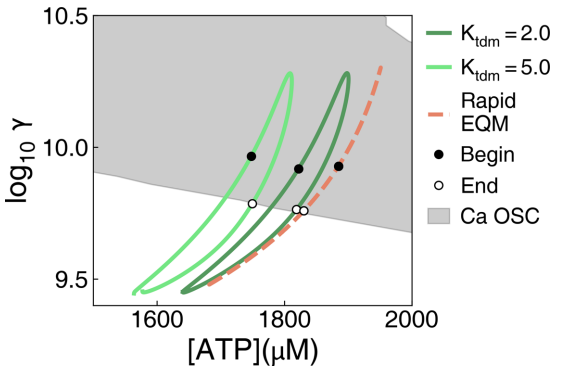

FIG. 17. The adenylate kinase related reaction constant ($K_{\rm tdm}$) affects the ATP trajectory, under $[A_{\rm tot}] = 2$ mM and [Glu] = 8 mM. Rapid equilibrium ("Rapid EQM") stands for the trajectory of the glycolysis model with the rapid equilibrium assumption for the adenylate kinase relevant reaction. The black and white points stand for the specific values of [ATP] and γ where the fast calcium oscillation begins and ends, respectively. The gray area represents the ATP range of fast calcium oscillation, which is computed by the ATP-constant two-variable model.

model, and its stochastic equation is formulated as

$$x_i(t+dt) = x_i(t) + f_i(\vec{x}(t))dt + \delta\alpha\sqrt{|f_i(\vec{x}(t))|dt},$$

where $dt = 2$ ms and is the time interval; $\vec{x}$ is the array of all variables; $f_i(\vec{x})$ is the ordinary differential equation of x_i in the glycolysis-calcium model; $\alpha = 0.02\sqrt{\mu\rm M}$ represents the relative noise level; δ is a normally distributed random variable and $\delta \sim N(0,1)$. We used Euler's method and the same parameters as in Table I to simulate the calcium response with noise, shown in Fig. 16(c).

We now discuss how the adenylate kinase reaction affects the ATP-γ trajectory. In Fig. 17, since the equilibrium constant of 2ADP $\leftrightarrow$ ATP + AMP was changed from 2 to 5, the ATP trajectory moved out of the fast oscillation region, with smaller mean [ATP]. In the IOM model [10], this reaction is introduced with rapid equilibrium conditions ($v_{ak} = 0$) and then

$$[\rm AMP] = \frac{[\rm ADP]^2}{K[\rm ATP]}.$$

Since the definition of $A_{\rm tot} = [\rm ATP] + [\rm ADP] + [\rm AMP]$, [ADP] and [AMP] are formulated as

$$[\rm ADP] = A_{\rm tot} - [\rm ATP] - [\rm AMP],$$
$$[\rm AMP] = A_{\rm tot} - [\rm ATP]/2 - \sqrt{(2A_{\rm tot} - [\rm ATP])^2 - 4([\rm ATP] - A_{\rm tot})^2}/2.$$

The equation of ATP and ADP, Eq. (6) in the glycolysis model, is now rewritten as

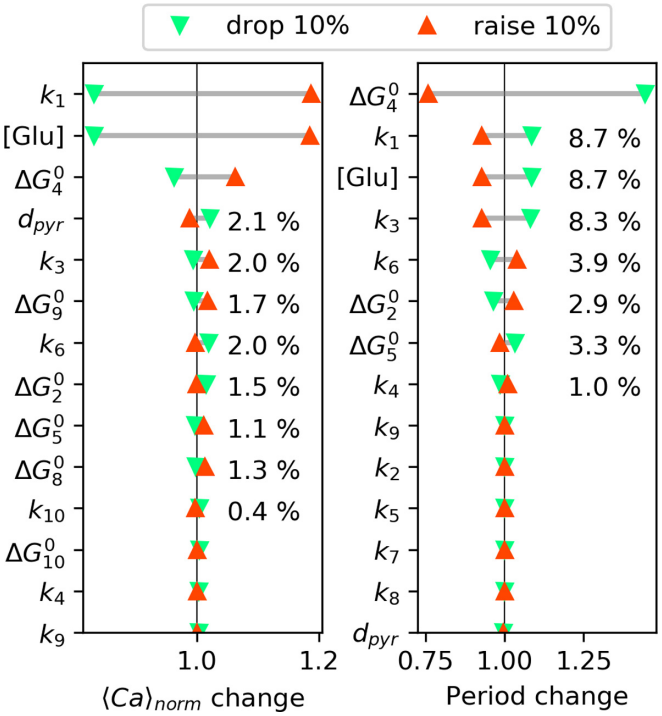

FIG. 18. Parameter sensitivity analysis of the glycolysis-calcium model. [Glu] = 8 mM and $[A_{\rm tot}] = 2$ mM. The standard score function $\langle \rm Ca\rangle_0 = 0.299$, and the standard period of ATP oscillation $P_0 = 7.28$ min. $\langle \rm Ca\rangle_{\rm norm}$ and period changes are defined as $\langle \rm Ca\rangle_{\rm norm}/\langle \rm Ca\rangle_0$, and P/P_0, where $\langle \rm Ca\rangle_{\rm norm}$ and P are the score function and period with a perturbed parameter set. Parameters are ranked by the change rate of score function or the period.

$$\frac{d[\rm ATP]}{dt} = -\frac{d[\rm ADP]}{dt} = -v_1 - v_3 + v_7 + v_9 + v_{\rm atp} - J^{\rm atp}_{\rm pmca}.$$

The numerical simulation in Fig. 17 shows that the trajectory changes from a circle to a curve, while it maintains the free energy level and moves slightly right in the ATP-γ space. It suggests that the rapid equilibrium assumption of the adenylate kinase relevant reaction shares the same results as our glycolysis-calcium model.

APPENDIX J: SENSITIVITY ANALYSIS OF PARAMETERS IN GLYCOLYSIS-CALCIUM MODEL

Parameter sensitivity analysis (see Fig. 18) was performed on the positive rates and the standard free energy of glycolysis reactions. We calculated the change ratio of $\langle$ Ca$\rangle_{\rm norm}$ and ATP oscillation period (slow mode) with a shift of each parameter by 10% or −10%. The standard $[A_{\rm tot}]$ and [Glu] were 2 and 8 mM, since this condition results in the most common response mode, *Type 1*. The glucose intake reaction (k_1 and [Glu]) plays the critical roles in cell response and ATP oscillation period. The FBP related reaction relevant parameters, k_3 and ΔG^0_4, are both important in the period, while ΔG^0_4 also influences the cell response.

[1] D. A. Beard and H. Qian, *Chemical Biophysics: Quantitative Analysis of Cellular Systems*, Cambridge Texts in Biomedical Engineering (Cambridge University Press, Cambridge, 2008).

[2] Y. Cao, H. Wang, Q. Ouyang, and Y. Tu, The free energy cost of accurate biochemical oscillations, Nat. Phys. **11**, 772 (2015).

[3] X. Yang, M. Heinemann, J. Howard, G. Huber, S. Iyer-Biswas, G. Le Treut, M. Lynch, K. L. Montooth, D. J. Needleman, S. Pigolotti, J. Rodenfels, P. Ronceray, S. Shankar, I. Tavassoly, S. Thutupalli, D. V. Titov, J. Wang, and P. J. Foster, Physical bioenergetics: Energy fluxes, budgets, and constraints in cells, Proc. Natl. Acad. Sci. USA **118**, e2026786118 (2021).

[4] H. Qian, Y.-C. Cheng, and Y.-J. Yang, Kinematic basis of emergent energetics of complex dynamics, Europhys. Lett. **131**, 50002 (2020).

[5] D. G. Nicholls, The pancreatic β-cell: A bioenergetic perspective, Physiol. Rev. **96**, 1385 (2016).

[6] P. Rorsman and F. M. Ashcroft, Pancreatic β-cell electrical activity and insulin secretion: Of mice and men, Physiol. Rev. **98**, 117 (2018).

[7] R. Bertram, L. S. Satin, and A. S. Sherman, Closing in on the mechanisms of pulsatile insulin secretion, Diabetes **67**, 351 (2018).

[8] I. Marinelli, B. M. Thompson, V. S. Parekh, P. A. Fletcher, L. Gerardo-Giorda, A. S. Sherman, L. S. Satin, and R. Bertram, Oscillations in K(ATP) conductance drive slow calcium oscillations in pancreatic β-cells, Biophys. J. **121**, 1449 (2022).

[9] M. C. Beauvois, C. Merezak, J. C. Jonas, M. A. Ravier, J. C. Henquin, and P. Gilon, Glucose-induced mixed $[Ca^{2+}]_c$ oscillations in mouse β-cells are controlled by the membrane potential and the SERCA3 Ca^{2+}-ATPase of the endoplasmic reticulum, Am. J. Physiol.: Cell Physiol. **290**, C1503 (2006).

[10] I. Marinelli, Theodore Vo, L. Gerardo-Giorda, and R. Bertram, Transitions between bursting modes in the integrated oscillator model for pancreatic β-cells, J. Theor. Biol. **454**, 310 (2018).

[11] G. J. Félix-Martínez, J. R. Godínez-Fernández, G. J. F. Elix-Mart Inez, and R. God Inez-Fern Andez, Mathematical models of electrical activity of the pancreatic β-cell: A physiological review, Islets **6**, e949195 (2014).

[12] T. Nilsson, V. Schultz, P.-O. Berggren, B. E. Corkey, and T. Tornheim, Temporal patterns of changes in ATP/ADP ratio, glucose 6-phosphate and cytoplasmic free Ca^{2+} in glucose-stimulated pancreatic β-cells, Biochem. J. **314**, 91 (1996).

[13] L. E. Fridlyand, L. Ma, L. H. Philipson, L. H. Philipson Adenine, and L. H. Philipson, Adenine nucleotide regulation in pancreatic-cells: modeling of ATP/ADP-Ca^{2+} interactions, Am. J. Physiol. Endocrinol. Metab. **289**, E839 (2005).

[14] S. J. Tucker, F. M. Gribble, P. Proks, S. Trapp, T. J. Ryder, T. Haug, F. Reimann, and F. M. Ashcroft, Molecular determinants of KATP channel inhibition by ATP, Embo. J. **17**, 3290 (1998).

[15] R. Bertram, L. Satin, M. Zhang, P. Smolen, and A. Sherman, Calcium and glycolysis mediate multiple bursting modes in pancreatic islets, Biophys. J. **87**, 3074 (2004).

[16] H. Qian, Phosphorylation energy hypothesis: Open chemical systems and their biological functions, Annu. Rev. Phys. Chem. **58**, 113 (2007).

[17] W. F. Hopkins, S. Fatherazi, B. Peter-Riesch, B. E. Corkey, and D. L. Cook, Two sites for adenine-nucleotide regulation of ATP-sensitive potassium channels in mouse pancreatic β-cells and HIT cells, J. Membr. Biol. **129**, 287 (1992).

[18] R. E. Plant, The effects of calcium $+ +$ on bursting neurons. A modeling study, Biophys. J. **21**, 217 (1978).

[19] D. Levy, M. Seigneuret, A. Bluzat, and J. L. Rigaud, Evidence for proton countertransport by the sarcoplasmic reticulum Ca^{2+}-ATPase during calcium transport in reconstituted proteoliposomes with low ionic permeability, J. Biol. Chem. **265**, 19524 (1990).

[20] T. R. Chay and J. Keizer, Minimal model for membrane oscillations in the pancreatic beta-cell, Biophys. J. **42**, 181 (1983).

[21] G. Magnus and J. Keizer, Model of β-cell mitochondrial calcium handling and electrical activity. I. Cytoplasmic variables, Am. J. Physiol.: Cell Physiol. **274**, C1158 (1998).

[22] G. Inesi, Sequential mechanism of calcium binding and translocation in sarcoplasmic reticulum adenosine triphosphatase, J. Biol. Chem. **262**, 16338 (1987).

[23] M. Schell, K. Kundu, and J. Ross, Dependence of thermodynamic efficiency of proton pumps on frequency of oscillatory concentration of ATP, Proc. Natl. Acad. Sci. USA **84**, 424 (1987).

[24] Y.-J. Liu, A. Tengholm, E. Grapengiesser, B. Hellman, and E. Gylfe, Origin of slow and fast oscillations of Ca^{2+} in mouse pancreatic islets, J. Physiol. **508**, 471 (1998).

[25] J. Li, H. Y. Shuai, E. Gylfe, and A. Tengholm, Oscillations of sub-membrane ATP in glucose-stimulated beta cells depend on negative feedback from Ca^{2+}, Diabetologia **56**, 1577 (2013).

[26] M. Matsuo, N. Kioka, T. Amachi, and K. Ueda, ATP binding properties of the nucleotide-binding folds of SUR1*, J. Biol. Chem. **274**, 37479 (1999).

[27] C. Z. Jin, X. D. Yan, and F. T. Li, Non-equilibrium and stochasticity influence the activation process of the yeast DNA damage pathway, Sci. China Phys. Mech. Astron. **61**, 028721 (2018).

[28] R. Yang, *Principles of Biochemistry*, Chinese edition (Higher Education Press, Beijingm 2006), pp. 372–393.

[29] D. L. Nelson and M. M. Cox, *Lehninger Principles of Biochemistry: International Edition*, 7th ed. (W. H. Freeman, San Francisco, 2017), pp. 534–548.

[30] T. Pipatpolkai, S. Usher, P. J. Stansfeld, and F. M. Ashcroft, New insights into K_{ATP} channel gene mutations and neonatal diabetes mellitus, Nat. Rev. Endocrinol. **16**, 378 (2020).

[31] A. I. Tarasov, T. J. Nicolson, J.-P. Riveline, T. K. Taneja, S. A. Baldwin, J. M. Baldwin, G. Charpentier, J.-F. Gautier, P. Froguel, M. Vaxillaire, and G. A. Rutter, A rare mutation in ABCC8/SUR1 leading to altered ATP-sensitive K^+ channel activity and β-cell glucose sensing is associated with type 2 diabetes in adults, Diabetes **57**, 1595 (2008).

[32] C. E. Amara, E. G. Shankland, S. A. Jubrias, D. J. Marcinek, M. J. Kushmerick, and K. E. Conley, Mild mitochondrial uncoupling impacts cellular aging in human muscles in vivo, Proc. Natl. Acad. Sci. USA **104**, 1057 (2007).

[33] Y. Ohta, A. Taguchi, T. Matsumura, H. Nakabayashi, M. Akiyama, K. Yamamoto, R. Fujimoto, R. Suetomi, A. Yanai, K. Shinoda, and Y. Tanizawa, Clock gene dysregulation induced by chronic ER stress disrupts β-cell function, EBioMedicine **18**, 146 (2017).

[34] L. Li, A. Trifunovic, M. Köhler, Y. Wang, J. P. Berglund, C. Illies, L. Juntti-Berggren, N.-G. Larsson, and P.-O. Berggren,Defects in β-cell Ca^{2+} dynamics in age-induced diabetes, Diabetes **63**, 4100 (2014).

[35] C. J. Barker, L. Li, M. Köhler, and P.-O. Berggren, β-cell Ca^{2+} dynamics and function are compromised in aging, Adv. Biol. Regul. **57**, 112 (2015).

[36] T. Wang, J. Zhao, Q. Ouyang, H. Qian, Y. V. Fu, and F. Li, Phosphorylation energy and nonlinear kinetics as key determinants for G2/M transition in fission yeast cell cycle, arXiv:1610.09637.

[37] H. Ren, Y. Li, C. Han, Y. Yu, B. Shi, X. Peng, T. Zhang, S. Wu, X. Yang, S. Kim, L. Chen, and C. Tang, Pancreatic α and β cells are globally phase-locked, Nat. Commun. **13**, 3721 (2022).

[38] D. Enkvetchakul, G. Loussouarn, E. Makhina, and C. G. Nichols, ATP interaction with the open state of the KATP channel, Biophys. J. **80**, 719 (2001).

[39] N. Vedovato, F. M. Ashcroft, and M. C. Puljung, The nucleotide-binding sites of SUR1: A mechanistic model, Biophys. J. **109**, 2452 (2015).

[40] S. G. Miller, P. S. Hafen, and J. J. Brault, Increased adenine nucleotide degradation in skeletal muscle atrophy, Int. J. Mol. Sci. **21**, 88 (2019).

[41] D. T. Gillespie, Stochastic simulation of chemical kinetics, Annu. Rev. Phys. Chem. **58**, 35 (2007).

[42] G. Dupont, M. Falcke, V. Kirk, and J. Sneyd, *Models of Calcium Signalling*, Interdisciplinary Applied Mathematics (Springer, Berlin, 2016), Vol. 43.

[43] R. L. Veech, J. W. Lawson, N. W. Cornell, and H. A. Krebs, Cytosolic phosphorylation potential, J. Biol. Chem. **254**, 6538 (1979).

[44] K. R. Albe, M. H. Butler, and B. E. Wright, Cellular concentrations of enzymes and their substrates, J. Theor. Biol. **143**, 163 (1990).